

## Observing The Hidden Sector

Bruce A. Campbell <sup>1,2</sup>, John Ellis <sup>2</sup> and David W. Maybury <sup>1</sup>

<sup>1</sup>*Department of Physics, Carleton University, 1125 Colonel By Drive,  
Ottawa ON K1S 5B6, Canada*

<sup>2</sup>*Theory Division, PH Department, CERN, CH-1211 Geneva 23, Switzerland*

### Abstract

We study the effects of renormalization due to hidden-sector dynamics on observable soft supersymmetry-breaking parameters in the minimal supersymmetric extension of the Standard Model (MSSM), under various hypotheses about their universality at a high input scale. We show that hidden-sector renormalization effects may induce the spurious appearance of unification of the scalar masses at some lower scale, as in mirage unification scenarios. We demonstrate in simple two-parameter models of the hidden-sector dynamics that the parameters may in principle be extracted from experimental measurements, rendering the hidden sector observable. We also discuss the ingredients that would be necessary to carry this programme out in practice.

# 1 Introduction

The most problematic aspect of supersymmetric phenomenology is the mechanism whereby supersymmetry is broken. The scenario usually adopted is that supersymmetry is broken in some ‘hidden’ sector that is (almost) decoupled from the observable sector [1, 2, 3, 4, 5]. It is often suggested, primarily for reasons of simplicity, that supersymmetry breaking is universal at some high input renormalization scale, perhaps the scale of grand or string unification [6]. This scenario, known as the CMSSM, is certainly simple, but it is not necessarily favoured by specific models of the dynamics in the hidden sector.

When relating this or any other scenario for supersymmetry breaking to low-energy phenomenology, it has usually been assumed that the renormalization of the effective soft supersymmetry-breaking parameters of the MSSM may be calculated reliably using the renormalization-group equations (RGEs) of the MSSM, neglecting the dynamics of the hidden sector. However, it was recently pointed out [7, 8, 9] that this may not be the case, and that the renormalization of the observable-sector supersymmetry-breaking parameters may be sensitive also to the hidden-sector dynamics [10]. The bad news is that this sensitivity introduces additional ambiguity into the low-energy predictions of even the CMSSM: the good news is that this sensitivity may enable experiment to provide some insight into the mechanism of supersymmetry breaking, even if it is ‘hidden’, and thought previously to be inaccessible to experimental probes. Thus, even the hidden sector may be observable.

We address this possibility in the context of supersymmetric theories with gauge coupling unification at a unification scale  $M_X$ . For simplicity, we further assume that supersymmetry breaking is mediated to the observable sector at a (high) scale  $M$  that is at least as large as the unification scale (this is the case in gravitational/moduli mediation and in anomaly mediation, where the scale is typically of order the reduced Planck mass). The latter assumption is not essential to our argument, and variants of our proposal can be adapted to lower-scale mediation mechanisms such as gauge mediation.

We show in this paper how, in a simple but general parametrization of the hidden sector model, low-energy measurements may be used, in principle, to extract information about the hidden sector. We work out in detail in this paper the reconstruction of the

hidden sector in models with the following two parameters: the dynamical scale  $M_{Hid}$  of the hidden sector, which is the infrared cutoff of the hidden sector running, and its effective interaction strength  $\lambda$  at the mediation scale. This particular parametrization has already been used previously in studies of hidden-sector effects [7, 8]. Further examples of calculations of the effects of the hidden sector in models parametrized in this way appear in a companion paper [11], which extends the discussion of this paper to seesaw models of neutrino masses and flavour mixing.

We adopt a renormalization scheme in which the hidden-sector external-line wavefunction renormalization of the singlet superfield  $S$  (whose F-term VEV is responsible for supersymmetry breaking) is absorbed into that VEV. The RGE evolutions of the gaugino masses are then unaffected by the hidden sector. However, the RGE evolutions of the supersymmetry-breaking scalar mass parameters also pick up one-particle-irreducible (1PI) contributions, and are in general modified by hidden-sector running down to the hidden-sector scale  $M_{Hid}$ , by an amount that depends on the effective interaction strength  $\lambda$ . As a result, the apparent scalar-mass unification scale that would, in our example, normally be inferred in the CMSSM from low-energy measurements is in general decreased below the true unification scale determined by the gauge couplings, approaching  $M_{Hid}$  in the limit of large  $\lambda$ . More generally, depending on the sign of the hidden-sector effects, the unification could also be ‘blown up’. The resulting distortion of the scalar spectrum is a characteristic of the hidden sector, which may be inverted to characterize general two-parameter models of the hidden-sector scalar-mass operator renormalization, giving information on the general structure of the hidden sector. This may be used to fit the two parameters of the hidden sector, and thereby render it ‘observable’, in a limited and indirect sense.

We give numerical examples of the modified RGE effects on different supersymmetry-breaking scalar mass parameters, and illustrate explicitly how low-energy measurements may be used to determine  $M_{Hid}$  and  $\lambda$ . Since there are many such mass parameters, namely  $m_{L,E^c,Q,U^c,D^c}$  for each of the three generations of sleptons and squarks, there is considerable redundancy in the determination of  $M_{Hid}$  and  $\lambda$ , and the universality assumed in the CMSSM can be tested in parallel.

In fact, as we discuss below, even if one assumes only that scalars with the same

gauge charges have the same mass at the unification scale (as is strongly indicated by the stringent limits on flavour-violating neutral interactions [12, 13, 15, 14]) then the interference of hidden-sector renormalization effects with observable-sector effects induced by the top-quark Yukawa coupling will allow one to fit the two parameters of the models of the hidden sector that we consider. If  $\tan\beta$  is sufficiently large for effects of the bottom Yukawa coupling on the RGE flow to be distinguishable, then an independent determination of the parameters in a two-parameter hidden sector model is possible. In general, comparison of these determinations will yield the same parameter values only if the parametrization in which the determination is done is one that correctly describes the qualitative behaviour of the hidden sector. If this is achieved, we would be able not only to select the correct hidden-sector parametrization, but also to determine the numerical values of its parameters.

In string constructions with gauge-coupling unification, there are often characteristic patterns of both the gaugino and scalar soft mass terms. For example, in F-theory constructions of unified theories with moduli mediation of flux breaking of supersymmetry, it has recently been argued that there is a simple pattern of soft gaugino terms, of soft scalar mass terms, and of A-terms, of the standard modulus-dominated type [16]. Similarly, in heterotic constructions of unified theories with uplifting via matter superpotentials, one typically sees a characteristic ‘mirage’ pattern for the soft terms, with the relative strength of the moduli contributions to the anomaly contributions governed by a single parameter  $\rho$  [17]. In different four-dimensional supersymmetric GUT models, various sets of relations between the input soft parameters are possible: for example, in supersymmetric SO(10) all the soft supersymmetric scalar masses would be equal, whereas in conventional SU(5) the masses of scalars in the  $\bar{\mathbf{5}}$  and  $\mathbf{10}$  representations would be different in general. In cases like these there are many relations between the soft parameters at the unification scale, which mean that there are many redundant checks on the choice and parameter values of a hidden-sector model, which can be fitted using the observed values of the soft parameters at low energy.

The organization of our paper is as follows. In Section 2 we review the detailed nature of the possible hidden-sector renormalization effects. In Section 3 we introduce simple generic families of two-parameter hidden-sector models parametrized by the nature of

the induced renormalization of the scalar mass operators. In Section 4 we demonstrate explicitly our proposed reconstruction in the case of a toy two-parameter hidden-sector model of the kind that was discussed in Section 3, but using a different parametrization taken from the existing literature, in order to facilitate the comparison of our results to those already extant. In Section 5 we discuss how one would undertake the proposed reconstruction starting with experimental data from the LHC and a future linear collider. Section 6 presents our conclusions. The Appendices list scalar-mass sum rules and the relevant RGEs.

## 2 Hidden-Sector Renormalization

In this section, we analyze the renormalization of operators that couple the hidden and CMSSM fields, as would result from strongly-coupled dynamics in the hidden sector [7, 9].

In general, there are both gauge non-singlet and singlet fields in the hidden sector, which we call  $F$  and  $S$ , respectively, without referring to particular models; they may be “elementary” or “composite”. We are interested in models where both the  $F$  and  $S$  fields may participate in strong-coupling dynamics, and hence their scaling properties may differ from their classical dimensions by potentially large anomalous dimensions. We refer generically to the chiral superfields of the CMSSM sector as  $\phi$ .

Direct couplings between the hidden and CMSSM fields arise from various local operators. These are higher-dimensional operators and suppressed by some energy scale  $M$ ; for the rest of this paper we will assume that this mediation scale  $M$  is at least of the order of the unification scale of the underlying theory (this is generically true in models of gravity, modulus or anomaly mediation). Analyses similar to that in this paper may be undertaken in mediation models with a lower scale, such as models of gauge mediation.

Some of the direct interaction operators are quadratic in the hidden sector fields. For example, operators that contribute to the scalar squared masses are

$$\mathcal{O}_\phi : \quad \int d^4\theta c_\phi^F \frac{F^\dagger F}{M^2} \phi^\dagger \phi, \quad \int d^4\theta c_\phi^S \frac{S^\dagger S}{M^2} \phi^\dagger \phi. \quad (1)$$

Other quadratic operators are

$$\mathcal{O}_{B\mu} : \quad \int d^4\theta c_{B\mu}^F \frac{F^\dagger F}{M^2} H_u H_d + \text{h.c.}, \quad \int d^4\theta c_{B\mu}^S \frac{S^\dagger S}{M^2} H_u H_d + \text{h.c.}, \quad (2)$$

that contribute to the  $B\mu$  parameter, the bilinear holomorphic supersymmetry-breaking parameter with dimension mass squared, that appears in the Higgs sector. Since we have scaled out powers of the mediation scale  $M$ , the coefficients  $c^i$  in (1, 2) are dimensionless.

There are also operators linear in the hidden-sector singlet fields. One example, for gauginos, is the mass operator

$$\mathcal{O}_\lambda : \quad \int d^2\theta c_\lambda^S \frac{S}{M} \mathcal{W}^{a\alpha} \mathcal{W}_\alpha^a + \text{h.c.}, \quad (3)$$

where the  $\mathcal{W}_\alpha^a$  ( $a = 1, 2, 3$ ) are the field-strength superfields for the Standard Model gauge group. The operators

$$\mathcal{O}_A : \quad \int d^4\theta c_A^S \frac{S}{M} \phi^\dagger \phi + \text{h.c.} \quad (4)$$

contribute to the  $A$  and  $B$  parameters, the parameters associated with holomorphic supersymmetry-breaking scalar trilinear and bilinear interactions, as well as the scalar masses  $|A|^2$ . And, the operator

$$\mathcal{O}_\mu : \quad \int d^4\theta c_\mu^S \frac{S^\dagger}{M} H_u H_d + \text{h.c.}, \quad (5)$$

contributes to the  $\mu$  parameter, the supersymmetric coupling between the two observable-sector Higgs supermultiplets.

In the above expressions we have used the formalism of global supersymmetry; since we wish to consider high-scale mediation mechanisms such as gravity/modulus and anomaly mediation, we require a formulation with local supersymmetry. To convert the previous expressions to be consistent with local supersymmetry, the terms integrated over a half of the superspace above must then include the conformal compensator field  $C$  as  $\int d^2\theta C^3$ , while the terms over the full superspace must include it a factor  $\int d^4\theta C^\dagger C$ . The latter should not be considered as part of the Kähler potential  $K$ , but rather as a factor in the the superspace density  $f = -3M_{\text{Pl}}^2 e^{-K/3M_{\text{Pl}}^2}$ , before the Weyl scaling that removes the field dependence in the Planck scale;  $M_{\text{Pl}}$  is the reduced Planck scale. After Weyl scaling, each chiral superfield should be further rescaled by  $1/C$  to obtain the canonical kinetic terms, leaving a nontrivial  $C$  dependence in the various mass parameters. In vacua with supersymmetry breaking and no cosmological constant,  $C = 1 + \theta^2 m_{3/2}$ , where  $m_{3/2}$  is the gravitino mass. Thus there is an implicit compensator dependence in all of the mass parameters, and sequestering (suppression) effects occur in  $f$ , not in  $K$ .

The wavefunction renormalization factor for the operators linear in the hidden-sector singlet field  $S$  is

$$\mathcal{L} = \int d^4\theta Z_S(\mu_R) S^\dagger S, \quad (6)$$

There are no 1PI diagrams that renormalize operators linear in  $S$ , and hence  $\mathcal{O}_\lambda$  in Eq. (3),  $\mathcal{O}_A$  in Eq. (4), and  $\mathcal{O}_\mu$  in Eq. (5) receive only the wavefunction renormalization  $Z_S^{-1/2}(\mu_R)$ .

In general, after external-line wave-function renormalization of the mediation operators linear in the hidden-sector singlet field, at an energy scale  $\mu_R$  below the scale of hidden-sector dynamics they take the form:

$$\int d^2\theta Z_S^{-1/2}(\mu_R) c_\lambda^S \frac{S}{M} \mathcal{W}^{\alpha\alpha} \mathcal{W}_\alpha^\alpha + \text{h.c.}, \quad (7)$$

for the gaugino masses,

$$\int d^4\theta Z_S^{-1/2}(\mu_R) c_A^S \frac{S}{M} \phi^\dagger \phi + \text{h.c.}, \quad (8)$$

for the  $A$ ,  $B$  parameters, and the  $|A|^2$  part of the scalar squared masses, and

$$\int d^4\theta Z_S^{-1/2}(\mu_R) c_\mu^S \frac{S^\dagger}{M} H_u H_d + \text{h.c.}, \quad (9)$$

for the  $\mu$  parameter.

Provided that there is a linear term in the superpotential, i.e. if there is an operator

$$\int d^2\theta f^2 S + \text{h.c.}, \quad (10)$$

where  $f$  has mass dimension one, the  $S$  field acquires an  $F$ -component VEV. In the basis where the  $S$  field is canonically normalized, this linear term is suppressed in the infrared as

$$\int d^2\theta Z_S^{-1/2}(\mu_R) f^2 S + \text{h.c.}. \quad (11)$$

The  $F$ -component VEV for the canonically-normalized  $S$  field is

$$F_S = -Z_S^{-1/2}(\mu_R) f^{*2} \quad (12)$$

and the vacuum energy is  $V_0 = |Z_S^{-1/2}(\mu_R) f^2|^2$ . Hence the gravitino mass is

$$m_{3/2} \approx Z_S^{-1/2}(\mu_R) \frac{|f|^2}{M_{\text{Pl}}}. \quad (13)$$

The wave function suppression  $Z_S^{-1/2}(\mu_R)$  of Eq. (13), however, also suppresses all the  $\mu$  and supersymmetry breaking parameters equally. For example, we find that the gaugino masses are given by

$$|M_a| \approx Z_S^{-1/2}(\mu_R) \frac{|c_\lambda^S F_S|}{M} = Z_S^{-1}(\mu_R) \frac{|c_\lambda^S f^2|}{M}, \quad (14)$$

where one factor of  $Z_S^{-1/2}(\mu_R)$  in this expression comes from that of Eq. (13), and the other  $Z_S^{-1/2}(\mu_R)$  from the suppression of the coefficient of Eq. (7). This latter  $Z_S^{-1/2}(\mu_R)$  provides a relative suppression of the gaugino masses relative to the gravitino mass:  $M_a/m_{3/2} \sim Z_S^{-1/2}(\mu_R)$  [9]. The same is also true for the  $\mu$  and  $A$  parameters, which are also linear in  $S$ .

In fact the extra relative factor of  $Z_S^{-1/2}(\mu_R)$  will appear with the corresponding superfield  $S$  in each of the mediation operators communicating soft supersymmetry breaking to the observable sector. As such, it can be affected by a constant rescaling of all the mediation operators with a factor  $Z_S^{-1/2}(\mu_R)$  for each  $S$  superfield. Since all soft masses arise from  $F_S$ , the  $S$ -field F-term, this represents a homogenous rescaling of all the terms in the RGE equations for the soft terms. If we rescale the input soft terms at the mediation scale  $M$  then, after the rescaling,  $O_A$ , and  $O_\mu$ , as well as  $O_\lambda$ , will all be unaffected by hidden-sector dynamics, as the net effect has been put into this rescaling. After this rescaling, we now see that the gravitino mass has an enhancement with respect to the the gaugino mass and the  $\mu$  and  $A$  parameters by a factor  $Z_S^{1/2}(\mu_R)$ . Apart from this homogenous rescaling of the input soft terms at the scale  $M$ , the quadratic operators  $O_\phi$  and  $O_{B\mu}$  also no longer receive corrections from the external line wave-function renormalization. However, being quadratic, the operators  $O_\phi$  and  $O_{B\mu}$  do receive extra renormalization due to the 1PI dynamical effects. These latter effects cannot be absorbed into a rescaling of the soft terms at  $M$ , and have observable physical consequences in the RGE flow of the soft supersymmetry-breaking parameters [8]. It is then physically important to determine the relative speed of suppression (sequestering) between the operators quadratic and linear in  $S$ . Let us assume that there is no mixing between those operators quadratic in  $S$  and those quadratic in  $F$ , and that only  $S$  has a supersymmetry-breaking VEV. If there were no extra contribution  $\alpha_S$  to the anomalous dimension of the operators from 1PI contributions to the hidden-sector renormalization of the operator, all the  $B\mu$  and

soft parameters would receive similar suppressions as  $M_a \sim \mu \sim A \propto Z_S^{-1/2} F_S$  and  $m_I^2 \sim B\mu \propto Z_S^{-1} F_S^2$ , while  $m_{3/2} \propto F_S$ . Here,  $m_I^2$  represent the supersymmetry breaking scalar squared masses.

In general, however, the situation is more intricate [9]. The operators of the form  $\mathcal{O}_\phi$  in Eq. (1) and  $\mathcal{O}_{B\mu}$  in Eq. (2) in general mix with each other, and the anomalous dimensions of the mediation operators bilinear in  $F$ , or  $S$ , receive non-zero corrections  $\alpha_{F,S}$  from 1PI hidden-sector renormalization. In this case, the suppression of the operators quadratic in  $S$  is controlled by the smallest eigenvalue of the  $2\gamma_i\delta_{ij} + \alpha_{ij}$  matrix, which we define as  $2\gamma_S + \hat{\gamma}_S$ . Here,  $i, j$  runs over  $F$  and  $S$ , and  $\gamma_F$ , and  $\gamma_S$  are the anomalous dimensions of the  $F$  and  $S$  fields. Note that, as we have defined it in the preceding equation,  $\hat{\gamma}_S$  represents the additional renormalization-group scaling that the least-suppressed quadratic operators receive, relative to the operators linear in  $S$ , due to their 1PI contributions, as well as their mixing with operators bilinear in  $F$ . An additional complication is that the operators quadratic in  $S$  also mix in a calculable way with the operators linear in  $S$ . In general, for the non-Higgs fields it is the combination  $c_\phi^S - |c_A^S|^2$  that is suppressed by the exponent  $2\gamma_S + \hat{\gamma}_S$  (after potentially mixing with other quadratic operators), and it is this combination of operators that contributes to the scalar masses-squared. Meanwhile, for the Higgs fields it is the combination  $c_\phi^S - |c_A^S|^2 - |c_\mu^S|^2$  that is suppressed by the same exponent, and it is this combination of operators that contributes to  $m_{H_{u,d}}^2 + \mu^2$ . The combination of operators that contributes to the  $B\mu$  parameter,  $c_{B\mu}^S - c_\mu^S(c_{A,H_u}^S + c_{A,H_d}^S)$ , is renormalized in the same way.

It is precisely the extra scaling of these eigenfunction combinations of the quadratic operators, parametrized by the  $\hat{\gamma}_S$ , whose effects we describe by general parametrizations in the next section, and whose effects, when combined with the observable-sector renormalization of the same operators, we show how to reconstruct from observable-sector masses and mixings.

In the case that one assumes a sufficiently large interval of RGE running to create a hierarchy between the magnitudes of the effects on the quadratic and the linear operators, one can obtain the following qualitatively different outcomes:

$$\begin{aligned} M_a^2 \sim \mu^2 \sim A^2 &\gg m_{Q_i,U_i,D_i,L_i,E_i}^2 \sim B\mu \sim m_{H_{u,d}}^2 + \mu^2 & (\hat{\gamma}_S > 0), \\ M_a^2 \sim \mu^2 \sim A^2 &\ll m_{Q_i,U_i,D_i,L_i,E_i}^2 \sim B\mu \sim m_{H_{u,d}}^2 & (\hat{\gamma}_S < 0), \end{aligned} \tag{15}$$

depending on the sign of the exponent  $\hat{\gamma}_S$ . (In the absence of the operator mixing,  $\hat{\gamma}_S = \alpha_S$ .) In addition, since the gravitino mass is generally enhanced by wave-function renormalization effects relative to all the soft parameters, it is also possible that anomaly mediation contributions may be a significant contribution to the low-energy soft supersymmetry-breaking parameters, giving rise to a mirage pattern of soft scalar mass terms. Although it is not possible to work out the signs or magnitudes of the exponents  $\hat{\gamma}_S$  for a given strongly-coupled theory with the currently available technology, theories of this class may be parametrized by their  $\hat{\gamma}_S$  values. In the next section we consider simple general parametrizations of the strongly-coupled hidden-sector dynamics in terms of these exponents  $\hat{\gamma}_S$ . The primary goal of this paper is to demonstrate that, in supersymmetric unified theories with strongly-coupled hidden sectors, the parameters and type of the hidden sector can be inferred from low-energy observables, at least for hidden sectors with simple two-parameter parametrizations.

Finally, we note that, whilst the quadratic operator 1PI renormalizations affect directly only the soft supersymmetry-breaking scalar mass-squared  $|M_\phi|^2$  and the  $B\mu$  parameters, under the RGE evolution due to observable-sector interactions these terms feed back into the other soft supersymmetry-breaking mass terms such as gaugino masses, at higher order.

### 3 Hidden-Sector Behaviour: General Parametrizations

As we discussed in the last section, after diagonalizing the anomalous-dimension mixing matrix for the quadratic hidden-sector scalar mass-squared terms, we find that the hidden-sector interactions responsible for generating the scalar and gaugino masses of the CMSSM take the generic forms,

$$\int d^4\theta k_i \frac{X^\dagger X}{M^2} \phi_i^\dagger \phi_i + \int d^2\theta c_\lambda^S \frac{S}{M} \mathcal{W}^{a\alpha} \mathcal{W}_\alpha^a + \text{h.c.}, \quad (16)$$

where  $X$  denotes the hidden-sector field corresponding to the dominant eigencombination

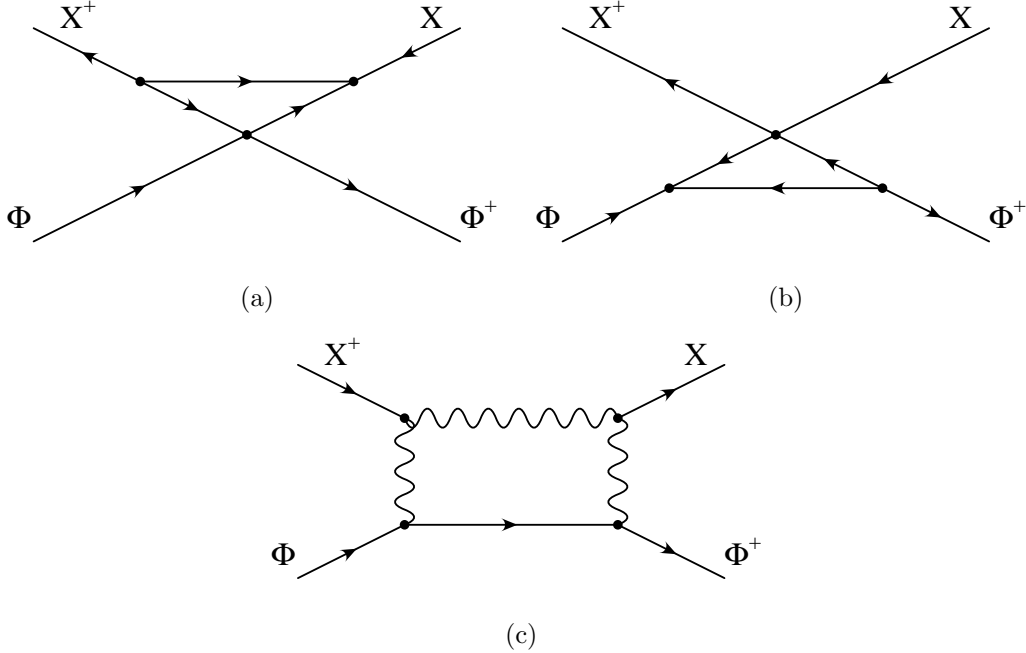


Figure 1: *One-loop supergraphs contributing to the soft supersymmetry-breaking scalar mass renormalization.*

of the  $F$  and  $S$ , generically the one with the smallest  $\hat{\gamma}_S$ <sup>1</sup>,  $k_i$  corresponds to the combination of  $c_\phi^F$  and  $c_\phi^S$  corresponding to the linear combination of  $F$  and  $S$  that composes the dominant eigencombination  $X$  (technically it is the largest  $k_i X^\dagger X$  that determines which is the dominant eigencombination for the purposes of keeping the dominant operator whose scaling we wish to consider),  $M$  represents the messenger scale, and  $\phi_i$  and  $\mathcal{W}_\alpha^a$  denote the visible-sector scalar and gaugino fields. As we see in Fig. 1, both the hidden- and visible-sector interactions renormalize the coefficients  $k_i$  and, since the  $k_i$  coefficients are responsible for setting the observable-sector soft supersymmetry-breaking scalar masses-squared in the CMSSM, the hidden sector can have an important impact on the final spectrum of scalars predicted at low energies. As a simple illustrative and analytic example, the one-loop contribution to the renormalization of  $k_i$  involving the hidden and gauge sectors yields [8] (we consider observable-sector superpotential interactions

<sup>1</sup>In exceptional cases, if the 1PI hidden-sector renormalization is weak and there is a larger initial value for a linear eigencombination corresponding to a larger value of  $\hat{\gamma}_S$ , the large initial value may overwhelm the scaling suppression, implying that the more suppressed eigencombination survives as the dominant eigencombination, in which case it would be that combination we label as  $X$ .

later),

$$\frac{d}{dt}k = \gamma(t)k_i - \frac{1}{16\pi^2} \sum_n 8C_2^n(R_i)g_n^6(t)G, \quad (17)$$

where  $\gamma(t)$  ( $\equiv \hat{\gamma}_S(t)$ ) denotes the anomalous dimension arising from the hidden-sector interactions in a hidden-sector renormalization scheme where we have removed the external-line wave-function renormalization of the  $S$  field by a rescaling of the soft supersymmetry-breaking mass terms, as discussed in the previous section, and the second term represents the leading visible-sector contribution containing the representation-dependent factors  $C_2(R_i)$  and gauge couplings,  $g_n$ . The solution to eq.(17) is

$$k_i(t) = \exp\left(-\int_t^0 dt' \gamma(t')\right) k_i(0) + \frac{1}{16\pi^2} \sum_n 8C_2^n(R_i) \int_t^0 ds g_n^6(s) \exp\left(-\int_t^s dt' \gamma(t')\right) G. \quad (18)$$

At this point, if we wish to study a particular model of the hidden sector, we may simply input it into the solution eq.(18) along with the running of the observable-sector gauge couplings.

However, it is useful to parametrize the general types of behaviour that may arise in hidden-sector effects on the RGE flow of the scalar masses. Since we wish to infer the nature of the hidden sector from the indirect effect it has on the flow of observable sector masses, through hidden-sector contributions to the operator RGE flow, in the presence of large observable-sector RGE contributions (gauge couplings,  $t$  Yukawa, possibly  $b$  and  $\tau$  Yukawas), we would expect that, in order for the hidden-sector effects to be noticeable, the hidden-sector coupling should become large somewhere in the range of running. Generally, one then expects a large contribution either at the lower range of running (near  $M_{hid}$ ), or at the upper range of running (near  $M$ , the messenger scale), or an approximately constant (scale-invariant) contribution over the range between  $M_{hid}$  and  $M$ . Furthermore, the sign of the effect on the operator will, in general, not be correlated with the apparent  $\beta$ -function behaviour corresponding to growth in the ultraviolet or infrared, because the apparent running may be a product of the operator mixing that we discussed in the previous section. Each of these cases may be described approximately by a simple two-parameter parametrization first proposed in [18], which expresses  $\gamma(t)$  as

$$\gamma(t) = \frac{1}{b_\gamma(t - a_\gamma)} \quad (19)$$

where  $t = \ln(\mu/M)$ . This is similar to how we parametrize the observable-sector gauge interactions:

$$g_n^2(s) = \frac{1}{b_n(s - a_n)} \quad (20)$$

where, for example,  $a_s = \log(\Lambda_{QCD}/M)$  would yield the standard one-loop parametrization of the QCD coupling. This two-parameter ( $b_\gamma$  and  $a_\gamma$ ) representation of the hidden-sector renormalization effects permits a simple mathematical characterization of the full class of possible model behaviours described above (models with approximately scale-invariant effects from the hidden sector over the range of running have an even simpler parametrization, as we discuss below). For example, plugging into the general solution of our simple analytic example, we find that

$$\exp\left(-\int_t^s dt' \gamma(t')\right) = \left(\frac{t - a_\gamma}{s - a_\gamma}\right)^{1/b_\gamma}, \quad (21)$$

which allows us to write

$$k_i(t) = (t - a_\gamma)^{1/b_\gamma} \left[ (-a_\gamma)^{-1/b_\gamma} k_i(0) + \frac{1}{16\pi^2} \sum_n 8C_2^n(R_i) G \int_t^0 ds \left(\frac{1}{b_n(s - a_n)}\right)^3 (s - a_\gamma)^{-1/b_\gamma} \right]. \quad (22)$$

We are now in a position to study the qualitative behaviours of the different cases parametrized above.

**Case 0:**  $\gamma = 0$ .

This trivial case corresponds to a negligible hidden-sector effect. Only the usual visible sector renormalization of the CMSSM appears.

**Case 1:**  $b_\gamma = -1$ ,  $a_\gamma = 1$ .

For the case of  $b_\gamma = -1$ , the integral can be explicitly done and the solution becomes:

$$k_i(t) = (t - a_\gamma)^{-1} \left[ -a_\gamma k_i(0) + \frac{1}{16\pi^2} \sum_n 8C_2^n(R_i) \frac{G}{b_n^3} \left( \frac{a_n + a_\gamma}{2a_n^2} + \frac{1}{t - a_n} - \frac{a_\gamma - a_n}{2(t - a_n)^2} \right) \right]. \quad (23)$$

With  $a_\gamma = 1$  this case corresponds to IR-free renormalizations in the hidden sector with strong coupling effects (perhaps nonperturbative) at mediation scale  $M$ . The choice  $b_\gamma = -1$  represents an extreme situation in the sense that the evolution becomes slow (walking), which enhances the hidden-sector effect. This gives an IR mass suppression at  $t_{hid} = \ln(M_{hid}/M)$  (with the suppression occurring predominantly at scales near  $M$ ) and

can give rise to “mirage unification”, in which the scalar masses appear to unify at an intermediate scale. We return to this case in detail in Section 4.

**Case 2:**  $b_\gamma = -1$ ,  $a_\gamma = \log(M_{hid}/M)$ .

The analytic solution in this case is the same as in the preceding  $b_\gamma = -1$  case. But now because  $a_\gamma = \ln(M_{hid}/M)$  we have UV-free effective renormalizations in the hidden sector with effects that become nonperturbative at  $eM_{hid}$ . At the scale  $t_{np} = \ln(eM_{hid}/M)$  we get an IR mass enhancement (with the enhancement occurring predominantly at scales near  $M_{hid}$ ). In this case the unification of masses may become completely obscured as they “blow apart”.

**Case 3:**  $b_\gamma = 1$ ,  $a_\gamma = 1$ .

In the case  $b_\gamma = 1$ , the integral can be done explicitly, and the solution becomes:

$$k_i(t) = (t - a_\gamma) \left[ (-a_\gamma)^{-1} k_i(0) + \frac{1}{16\pi^2} \sum_n 8C_2^n(R_i) \frac{G}{b_n^3} \left[ \frac{1}{(a_\gamma - a_n)^3} \log \left( \frac{a_\gamma(t - a_n)}{a_n(t - a_\gamma)} \right) + \frac{1}{(a_\gamma - a_n)^2} \left( \frac{-1}{a_n} - \frac{1}{t - a_n} \right) + \frac{1}{2(a_\gamma - a_n)} \left( \frac{1}{a_n^2} - \frac{1}{(t - a_n)^2} \right) \right] \right]. \quad (24)$$

With  $a_\gamma = 1$  this case corresponds to IR-free renormalization in the hidden sector with strong-coupling effects (possibly nonperturbative) at the mediation scale  $M$ . Because of the negative sign of  $\gamma(t)$  in the regime of running, the masses are IR-enhanced (predominantly from scales near  $M$ ), which means that unification of masses could become obscured as they “blow apart”.

**Case 4:**  $b_\gamma = 1$ ,  $a_\gamma = \ln(M_{hid}/M)$ .

The analytic solution in this case is the same as in the preceding  $b_\gamma = 1$ , case. But now because  $a_\gamma = \ln(M_{hid}/M)$  we have UV-free effective renormalizations in the hidden sector with effects that become nonperturbative at  $M_{hid}$ . This gives an IR mass suppression at  $t_{hid} = \log(M_{hid}/M)$  (with the suppression occurring predominantly at scales near  $M_{hid}$ ) and can give rise to “mirage unification”, in which the scalar masses appear to unify at an intermediate scale.

For hidden sectors with approximately scale-invariant behaviour (somewhere) in the range between  $M_{hid}$ , the scale of spontaneous supersymmetry breaking in the hidden sector, and  $M$ , the mediation scale, it is easy to find simple two-parameter characterizations

of their behaviour. One parameter is clearly the (constant) value of  $\gamma$  over the scaling interval. The other parameter will govern the extent of the scaling interval; this will be a mass scale  $M_c$  that governs the limit of the region of approximately scale-invariant running. The scale-invariant region could be at the high end of the interval, starting at  $M$  and running down to  $M_c$ , or at the low end of the interval, starting at  $M_c$  and running down to  $M_{hid}$ . We leave to readers the exercise of working out the solution of our simple analytic example for hidden sectors parametrized by these behaviours.

With simple parametrizations of the potential behaviours of the hidden-sector contributions to the RGE running of the scalar masses, we may now turn to the question of their effect on the soft supersymmetry-breaking terms that could be measured at observable energies. Appendix A lists sum rules between the scalar masses that hold even in the presence of hidden-sector effects (see also [10]). In general, one needs to integrate numerically the full set of MSSM RGE equations (see Appendix B for these equations at one-loop order) with the addition of the hidden-sector scalar mass-squared anomalous-dimension terms as in (17), in a parametrization such as those proposed in this Section. In the next Section we consider the degree to which the resulting predictions for the soft supersymmetry-breaking parameters may be used to determine the type and parameters of the hidden sector that induced them, rendering the hidden sector ‘observable’.

## 4 Hidden-Sector Reconstruction

In this Section we consider how the effects of the hidden-sector renormalization, combined with that from observable-sector interactions, can cause observable distortions in the low-energy spectrum of the soft supersymmetry-breaking scalar mass-squared terms. We make minimal assumptions on the spectrum of the soft supersymmetry-breaking scalar mass-squared terms input at the unification scale. As a first example we assume a universal value for squark and slepton masses squared. Subsequently we relax this assumption, but keeping a common value for scalars with the same gauge charges, as seems to be required by the limits on neutral supersymmetric flavour violation [12, 13, 15, 14]. We show that, with these assumptions, we can in principle distinguish the general classes of two-parameter hidden-sector parametrizations introduced in the last Section, and re-

construct their parameters.

We illustrate this reconstruction using a two-parameter hidden sector of the type of Case 1 from the previous Section <sup>2</sup>. In order to facilitate the comparison to previous literature, we describe it differently. Following [7, 8] we consider a toy self-interacting hidden sector that contains the superpotential term

$$W_h = \frac{\lambda}{3!} X^3. \quad (25)$$

This simple superpotential by itself does not break supersymmetry, and hence the hidden sector of eq.(25) must be enlarged by additional interactions responsible for generating F- or D-term VEVs in a realistic model. For the purposes of examining the effects of hidden-sector renormalization, following [7, 8] we suppose that eq.(25) appears as the dominant self-interaction term in the hidden-sector superpotential, and that it provides the dominant hidden-sector contribution to the anomalous dimension of the operator mediating supersymmetry breaking scalar masses in the observable sector. The observable interactions generate the usual MSSM RGEs, while the separate hidden-sector renormalizations of the coefficients  $k_i$  of eq.(16) – resulting from the self-interactions in eq.(25) – add an additional contribution. The hidden-sector Yukawa interactions at lowest order in  $\lambda$  yield  $\gamma(t) = (2\lambda^*(t)\lambda(t))/(16\pi^2)$  where, as per our convention, we have removed the external-line wave-function contributions to the RGE running of the operator, and  $\lambda(t)$  is the running hidden-sector Yukawa coupling, which to lowest order satisfies:

$$\frac{d\lambda}{dt} = \frac{3}{32\pi^2} \lambda^3. \quad (26)$$

In line with the aim of this paper, and to facilitate comparison to the previous literature, we now define our (two-parameter) parametrization of this hidden sector. We use as our two parameters the value of the coupling  $\lambda$  at the unification scale and the value of the scale  $M_{hid}$  which gives the infrared cutoff on the hidden-sector dynamical scale. We consider this as variable, yielding a two-parameter toy model of the hidden sector. Finally, we define the leading-order expression  $\gamma(t) = (2\lambda^*(t)\lambda(t))/(16\pi^2)$  as the

---

<sup>2</sup>Readers can easily adapt our arguments to all the parametrizations of the different behaviours described in the previous section. Indeed, in a companion paper [11] we study neutrino seesaw physics with both this and several alternative parametrizations of hidden-sector behaviours.

exact value of the anomalous dimension  $\gamma(t)$ . This is clearly true only at leading order in the theory we wrote down in eq.(25), but it defines a convenient parametrization of the behaviour we wish to assume in our example, and it facilitates comparison to previous results which use the leading order expression. Similarly, for our numerical studies we use the leading-order RGE behaviour of the coupling  $\lambda$  as if it were exact. This yields a hidden-sector contribution to the running of  $k_i$  given by

$$\frac{dk_i}{dt} = \frac{2\lambda^*\lambda}{16\pi^2}k_i, \quad (27)$$

implying that the scalar mass RGEs of the MSSM become augmented between the unification and messenger scales, becoming:

$$\frac{d\mathbf{m}_S^2}{dt} \rightarrow \frac{d\mathbf{m}_S^2}{dt} + \frac{2\lambda^*\lambda}{16\pi^2}\mathbf{m}_S^2. \quad (28)$$

Again remembering our convention that we remove the external-line wave-function renormalization effect (i.e., we work as if the gaugino masses are held fixed under hidden-sector renormalization). We see in eq.(28) that the hidden-sector contribution is the same for all scalar mass-squared RGEs, and therefore the effect on the running of the scalar masses-squared depends on the representation of the scalar particle itself. This effect suggests a fully general strategy for uncovering the effects of the hidden sector on the low-energy spectrum.

We demonstrate this strategy with two examples, and then detail the general method of hidden-sector reconstruction. In our two examples, we consider the cubic superpotential for the hidden sector as given in eq.(25), yielding an infrared-free hidden sector  $\beta$ -function for the Yukawa coupling. We stress that this choice of the hidden sector represents a proof-of-principle example, chosen to facilitate comparison with the existing literature, and should not be considered as a realistic scenario.

## 4.1 Example 1: Universal Scalar Masses and Observable-Sector Gauge Interactions

In this first example, we also assume universal scalar masses and universal gaugino masses at the unification scale  $M_X \approx 2 \times 10^{16}$  GeV, and an intermediate hidden-sector scale. Also, we assume that all trilinear A-terms vanish at  $M_{Pl}$ , and we assume a positive

sign for  $\mu$ . Given these model assumptions, we now demonstrate that it is possible to reconstruct the parameters of the hidden sector using the observable low-energy scalar masses.

Since the effects of the hidden sector on the scalar masses-squared depend on the representations of the scalar particles, we first plot the running for two different species with the hidden sector turned on, and then extrapolate the low-energy result backward with the hidden sector turned off, so as to examine fully its effects. We see some typical results in Fig. 2, where we have assumed a universal scalar mass of 115 GeV and a universal gaugino mass of 375 GeV at  $M_X$ , and we have placed the hidden-sector scale  $M_{hid}$  (where we integrate the hidden sector out of the system) at  $10^{12}$  GeV. In Fig. 2 we run downward the RGEs of the masses-squared of the third-generation left-handed slepton,  $L_3$ , and of the third-generation right-handed slepton,  $l_3^c$ , using universal boundary conditions at  $M_X = 2 \times 10^{16}$  GeV, to yield low-energy predictions for the scalar masses-squared. The uppermost solid and dashed lines in Fig. 2 show the RGE evolution if the hidden-sector coupling  $\lambda$  vanishes. A naive extrapolation up from low energies using just the MSSM RGEs yields the correct result that the masses unify at  $M_X$ .

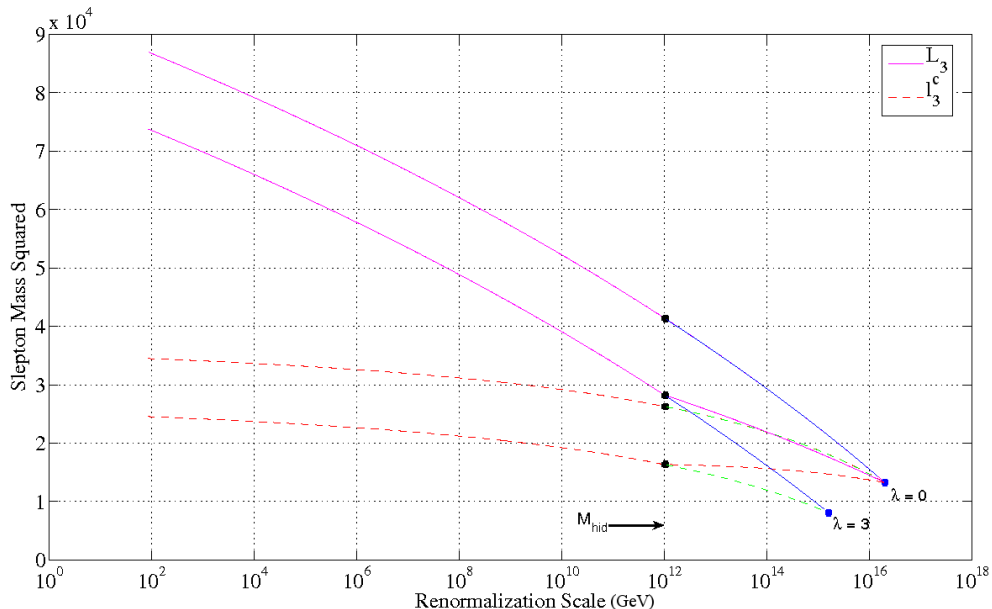


Figure 2: *The RGE flows of the largest mass-squared eigenvalues for the third-generation left ( $L_3$ ) and right-handed ( $l_3^c$ ) slepton for  $\lambda = 0$  and  $\lambda = 3$ .*

However, since the left- and right-handed sleptons sit in different representations of  $SU(2)_L$ , the RGE flows of the two scalar masses proceed differently between  $M_X$  and  $M_{hid}$  for non-zero  $\lambda$ , as shown by the middle solid and dashed lines in Fig. 2 that are present between  $M_X$  and  $M_{hid}$ . Using the low-energy predictions obtained from the theory with the hidden-sector effects incorporated to define the initial conditions at low energy, if we naively run the MSSM RGEs upward, neglecting the effect of the hidden sector (as shown by the lowest solid and dashed lines in Fig. 2), we see that the intersection of the  $L_3$  and  $l_3^c$  masses appears to take place at a scale different from  $M_X$  if  $\lambda$  is non-zero. That is, the hidden-sector effect predicts that the RGE flow of the usual MSSM applied naively to the observed low-energy scalar masses-squared of different representations will appear to yield “mirage unification” at a scale distinct from the gaugino unification point at  $M_X$  (which the hidden-sector effect leaves unaltered). The appearance of such a mirage scalar-unification scale would be the first indication of the presence of a hidden-sector effect <sup>3</sup>.

In Fig. 3 we plot the mirage scale as a function of predicted scalar mass at the low scale. Here we have used backward extrapolation to determine the intersection points for the pairs  $(L_3, l_3)$ ,  $(Q_3, u_3^c)$ , and  $(Q_1, u_1^c)$  for  $\lambda = 0-4$ . In all cases we have used the same MSSM inputs as in Fig. 2. We emphasize again that the mirage scale is a fake, in that it simply indicates the presence of additional structure relative to the pure weakly-coupled CMSSM scenario.

While Figs. 2 and 3 demonstrate how a mirage scale develops, by examining the RGE flow using the low-energy output of a particular high-energy implementation, empirically we will only have the low-energy spectrum – we will not know the scale at which to integrate out the hidden sector, nor will we know its Yukawa coupling  $\lambda$ . Thus, we require a complete bottom-up approach and an understanding of the level of parameter degeneracy in this system.

Under the assumption of universal scalar masses and a hidden sector given by eq.(25), a fixed universal scalar mass at  $m_0$  can lead to the same prediction for the low-energy scalar mass for different values of  $M_{hid}$  and  $\lambda$ . Furthermore, different values of  $m_0$  can lead to the same low-energy prediction by compensating different inputs with  $M_{hid}$  and

---

<sup>3</sup>For a phenomenological analysis of ‘mirage’ scenarios, see [19].

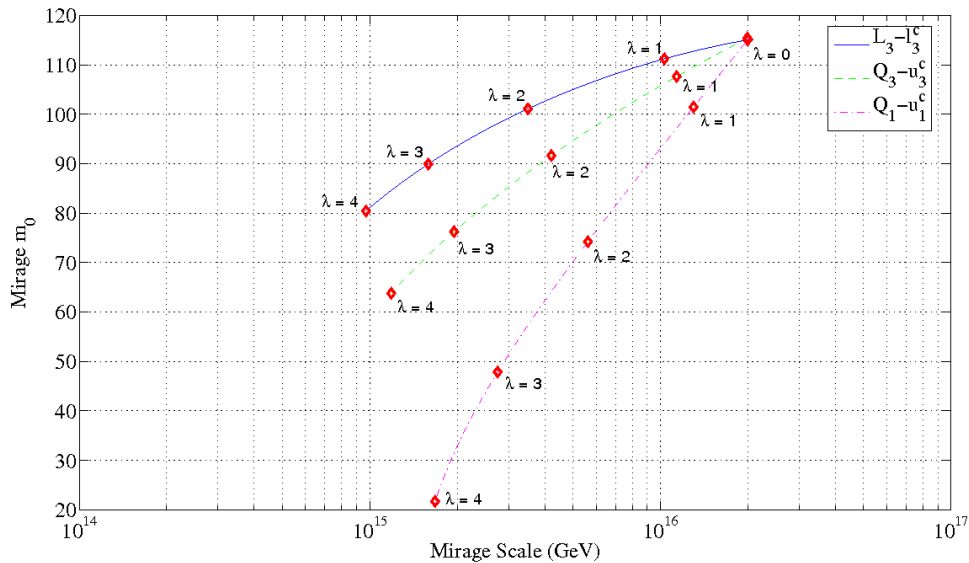


Figure 3: *The dependences of the mirage scale and the mirage scalar mass on  $\lambda$  for  $M_{\text{hid}} = 10^{12}$  GeV, using the same MSSM inputs as in Fig. 2.*

$\lambda^4$ . Fig. 4 demonstrates four different parameter choices that lead to the same predicted value for the largest left-handed slepton eigenvalue,  $m_{L_3} = 275$  GeV at the weak scale. This figure indicates that contours of constant  $m_0$  develop in the  $M_{\text{hid}} - \lambda$  plane, that lead to the same low-energy scalar mass prediction.

In Fig. 5 we show the effects of allowing  $M_{\text{hid}}$  and  $\lambda$  to vary while ensuring the same low-energy prediction of Fig. 4, namely  $m_{L_3} = 275$  GeV at the weak scale. Allowing  $m_0$  to range from 95 GeV to 135 GeV in 10 GeV increments, we produce five contours in the  $M_{\text{hid}} - \lambda$  plane as indicated by the dashed line in Fig. 5. We see that information on  $m_{L_3}$  alone is insufficient to determine the value of  $m_0$  or the hidden-sector parameters from low-energy data.

However, we can now consider a different particle species and generate a similar set of contours within the same theoretical framework. By overlaying the two sets of contours and searching for the line of intersection consistent with our model assumption of universal scalar masses, we can reduce the parameter degeneracy of Fig. 5. In Fig. 6, we perform

---

<sup>4</sup>Added complications appear if we do not assume total scalar universality, and we address this issue in our second example.

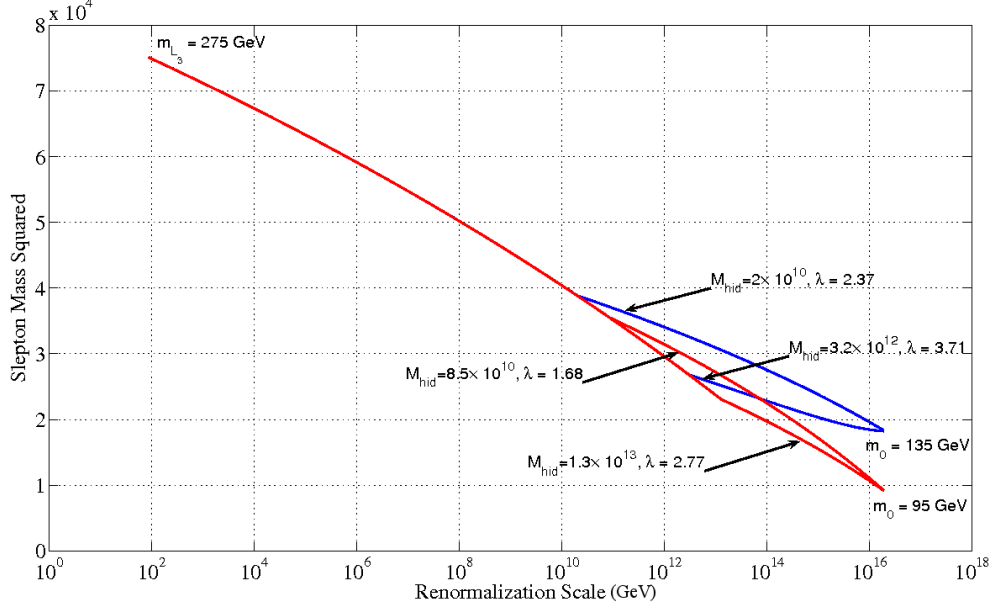


Figure 4: *Different choices of the hidden-sector parameters and the universal input scalar mass  $m_0$  can lead to the same low-energy prediction,  $m_{L_3} = 275$  GeV in this case.*

the same exercise as in Fig. 5, but considering this time the third-generation right-handed down squark, assuming  $m_{d_3^c} = 940$  GeV at the weak scale. In principle, we could take any species different from  $L_3$ , but by choosing the species most widely separated in gauge charges, we have a larger lever arm for obtaining the curve of intersection from the contour overlay.

We now take the contours of Fig. 5 and Fig. 6, and overlay them in Fig. 7. Under the assumption of universal scalar masses, the true theory must lie somewhere along the line of intersection indicated in the plot as a lighter (green) solid line. Whilst this line of intersection reduces the parameter space, we still do not have enough information to uncover uniquely the parameters of the hidden sector or the universal scalar mass. However, we can repeat the process of contour overlaying with two different species, and remove the parameter degeneracy.

In Fig. 8 we superpose the third-generation left-handed squark, assuming  $Q_3 = 940$  GeV at the weak scale, and the third-generation right-handed slepton, assuming  $l_3^c = 160$  GeV at the weak scale. We notice again a curve of intersection in Fig. 8,

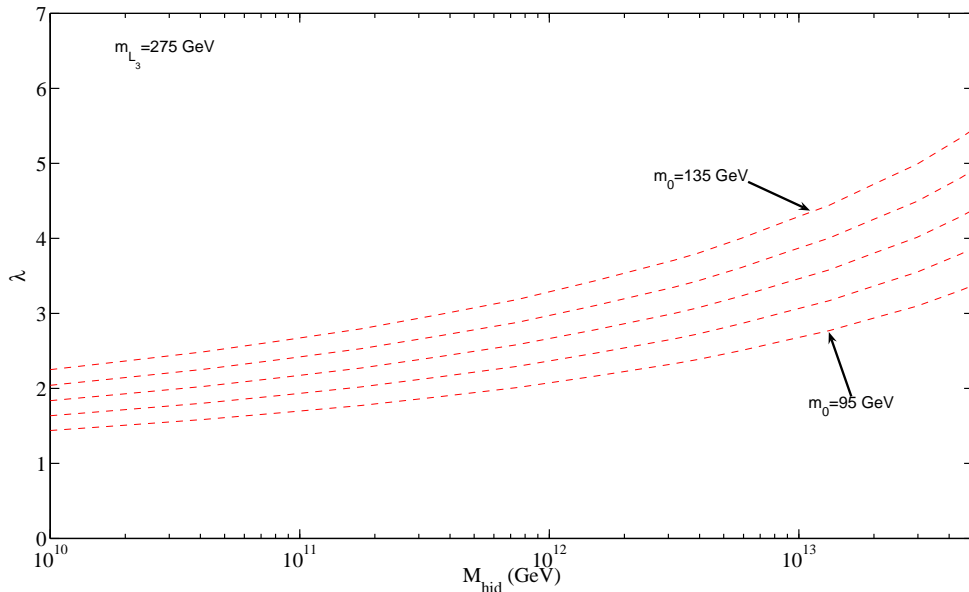


Figure 5: *For a fixed low-energy prediction of a slepton mass ( $m_{L_3} = 275$  GeV in this case), contours at different  $m_0$  exist in the  $M_{hid}-\lambda$  plane that predict the same low-energy mass value.*

denoting consistency with universal scalar masses.

We are now in a position to determine the parameters of the theory from the low-energy inputs. Having identified the curves of intersection of the contours using two different pairs of species (in this case  $L_3-d_3^c$  and  $Q_3-l_3^c$ ), we can now overlay the curves of intersection themselves. The crossing point of the two curves of intersection yields the unique point which determines both parameters of the hidden sector,  $M_{hid}$  and  $\lambda$ , along with the universal scalar mass  $m_0$ . We can see the result for this example in Fig. 9.

We note that the universal scalar mass behaves like an affine parameter along each intersection curve. A consistent theory of the hidden sector with the assumption of universal scalar masses not only requires that the intersection of the contour-intersection curves, but also that the intersection occurs at the same affine parameter – the universal scalar mass. As a consistency check on the method, we can repeat the process with yet another pair of species. Fig. 10 demonstrates the consistency check by repeating the process with the pair  $u_3^c-u_1^c$  and adding the third contour-intersection curve to figure 9.

Whilst the method demonstrated in Figs. 5 to 10 allowed us to reconstruct the hidden-

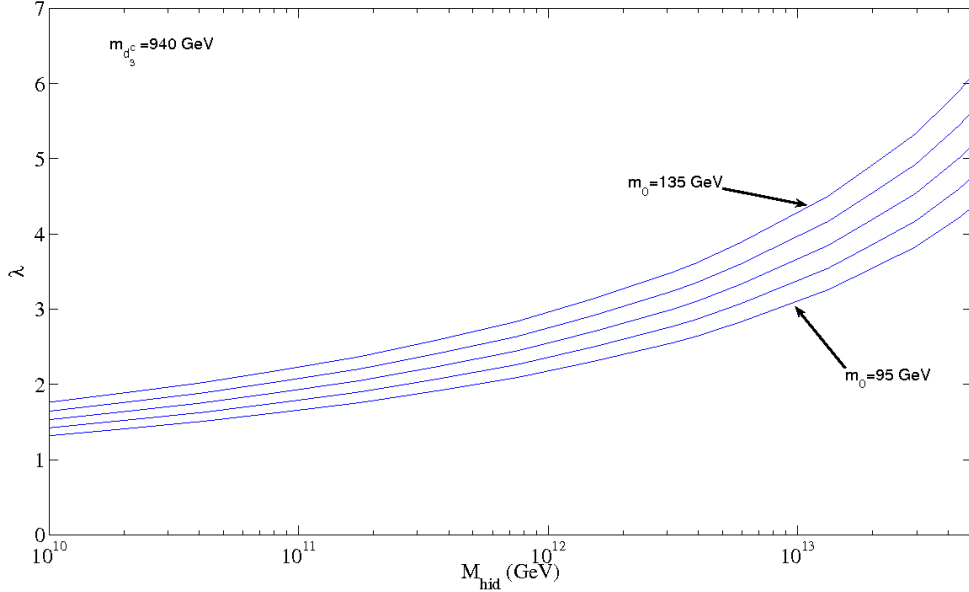


Figure 6: For a fixed low-energy prediction of a squark mass ( $m_{d_3^c} = 940$  GeV in this case), contours at different  $m_0$  exist in the  $M_{\text{hid}}-\lambda$  plane that predict the same low-energy mass value.

sector parameters and the visible sector  $m_0$ , we required certain model assumptions. First, we assumed that the visible sector contained totally universal scalar masses and secondly that the hidden sector could be described by a two-parameter model. Under these mild assumptions we showed that we could recover a consistent model. If the reconstruction outlined above failed to recover a unique point in a plot similar to Fig. 10, then we would know that at least one of the model assumptions was incorrect.

In principle there are fifteen different observable eigenvalues in the slepton/squark sector:  $L_{1,2,3}$ ;  $l_{1,2,3}^c$ ;  $Q_{1,2,3}$ ;  $u_{1,2,3}^c$ ;  $d_{1,2,3}^c$ . Only the third-generation Yukawa couplings are large enough to cause significant generational splitting, which reduces the observable list to seven effective eigenvalues:  $L_{(12)}$ ;  $L_3$ ;  $l_{(12)}^c$ ;  $l_3^c$ ;  $Q_{(12)}$ ;  $Q_3$ ;  $u_{(12)}^c$ ;  $u_3^c$ ;  $d_{(12)}^c$ ;  $d_3^c$ . The lightest eigenvalue in the up-like squark sector tracks the effect of the top Yukawa coupling, and if  $\tan \beta$  is large enough for the bottom and tau Yukawa couplings to be usefully large they will do likewise. With the 21 different possible pairings over-constraining the system, we can test model consistency, as illustrated in our example above.

On the other hand, the method outlined above is not restricted to models with total

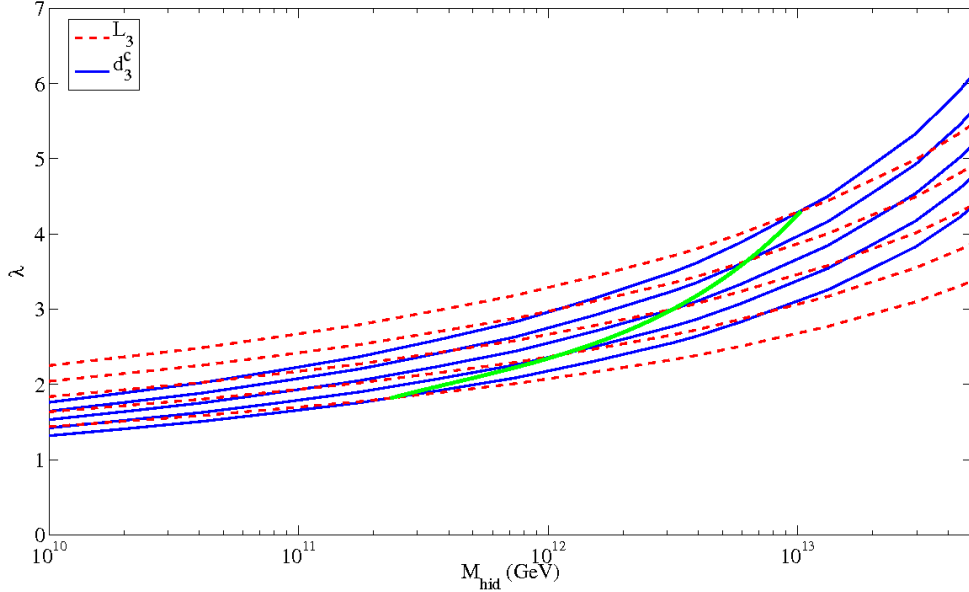


Figure 7: *Overlay of the contours in the  $M_{hid}$ - $\lambda$  plane of the largest-eigenvalue left-handed slepton from Fig. 5 (dashed lines) with those of the largest-eigenvalue right-handed squark from Fig. 6 (dark solid lines), assuming a universal soft supersymmetry-breaking scalar mass  $m_0$ . The intersections (linked by a lighter solid line) show how measurements of the two masses can be combined to determine the values of  $M_{hid}$  and  $\lambda$ .*

universality among the scalar masses. Results showing the absence of exotic contributions of flavour-changing neutral-current (FCNC) interactions in the kaon and B-meson system require a high level of mass degeneracy ( $\Delta m \lesssim 10^{-4}$ ) between scalar particles carrying the same gauge quantum numbers – the super-GIM mechanism. Even if we assume the least amount of universality consistent within the model class we consider by requiring all scalar particles with the same gauge quantum numbers appear with a common mass at  $M_X$ , we can still reconstruct the model parameters of the hidden sector. In this case, we can use the large third-generation Yukawas, that create generational splitting, to provide a lever arm for reconstructing the hidden-sector parameters. We demonstrate this reconstruction in our second example.

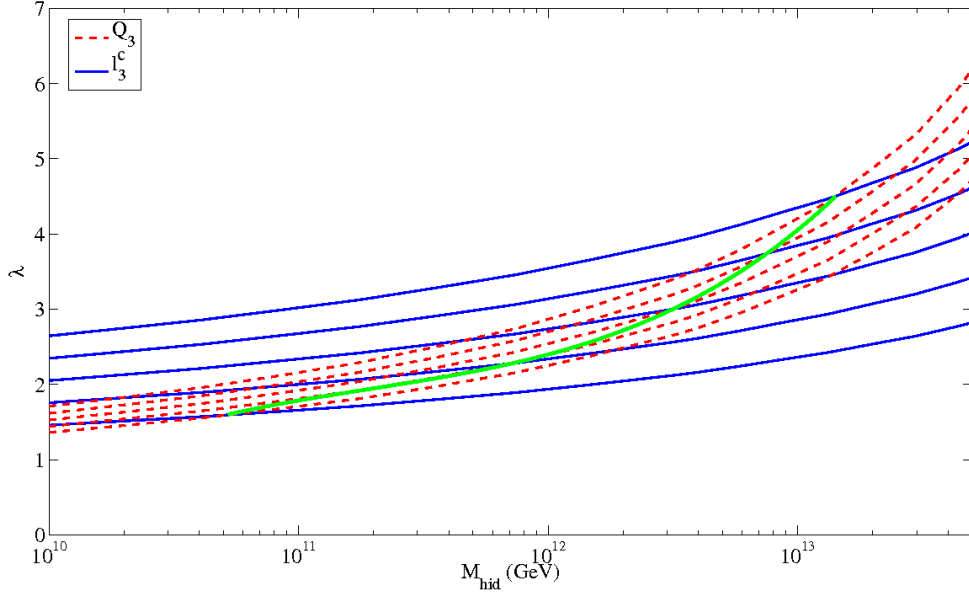


Figure 8: *As in Fig. 7, but overlaying contours of the largest-eigenvalue left-handed squark mass with contours of the largest-eigenvalue right-handed slepton mass, again assuming a universal soft supersymmetry-breaking scalar mass  $m_0$ .*

## 4.2 Example 2: Non-Degenerate Scalars and the Top Yukawa Coupling

We again assume a model of the hidden sector as given in eq.(25). However, in this example we assume a common mass only for squarks with the same gauge quantum numbers, namely  $Q_i(M_X) = m_0$  and  $u_i^c(M_X) = m'_0 \neq m_0$  in general. We then proceed analogously to the previous example, this time generating contours in the  $M_{hid}-\lambda$  plane for the  $Q_1 - Q_3$  and  $u_3^c - u_1^c$  systems. The differences between the contours are due to the top-quark Yukawa contributions to the RGEs for the third-generation squarks. In Fig. 11 we overlay the contours corresponding to different input soft supersymmetry-breaking masses for  $Q_3 - Q_1$ , and the lighter-coloured (green) solid line intersecting the contours corresponds to common values for the input mass. Repeating this process with the  $u_3^c - u_1^c$  system yields Fig. 12.

At this point, we overlay the two curves of intersection from Figs. 11 and 12, and examine the crossing point as shown in Fig. 13. We recall that we allow  $m'_0 \neq m_0$  in this

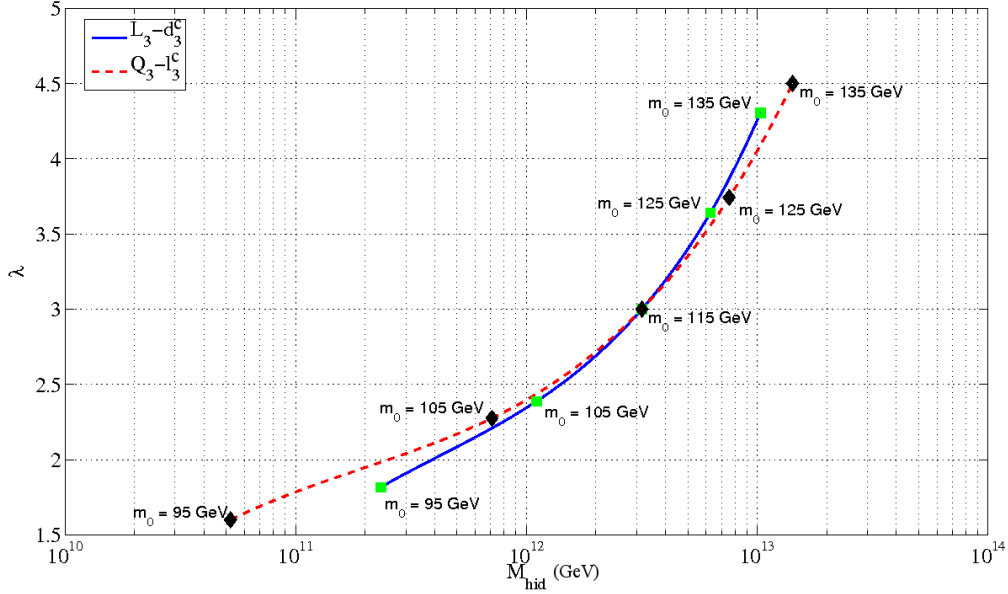


Figure 9: *The intersection of the intersection contours from Figs. 7 and 8 enables the parameters of the hidden sector to be reconstructed unambiguously from the low-energy data: the example chosen has  $m_0 = 115$  GeV,  $\lambda = 3$ , and  $M_{hid} = 3.16 \times 10^{12}$  GeV.*

example. We again see that we can extract the parameters of the hidden sector via the intersection point in the  $M_{hid} - \lambda$  plane. We recall that the visible sector parameter  $m_0$  serves as an affine parameter along each curve. Notice that in this case we obtain two different values for the visible sector parameter  $m_0$ , since the curves intersect at different values of their respective affine parameters. Thus, even in the more conservative case in which we assume a common scalar masses only among particles with the same gauge quantum numbers, consistent with a super-GIM mechanism, we can still reconstruct the parameters of the hidden sector by concentrating on the effects of the large Yukawa couplings.

With only the  $Q_1 - Q_3$  and  $u_1^c - u_3^c$  systems, we would not be able to discriminate between different models of the hidden sector. However, for sufficiently large  $\tan \beta$ , the third-generation down quark also has a large Yukawa coupling (and if  $\tan \beta$  is large enough we may be able to repeat the procedure with a large  $\tau$  Yukawa coupling). Then we can use the  $Q_1 - Q_3$  and  $d_1^c - d_3^c$  system, to get an independent determination of

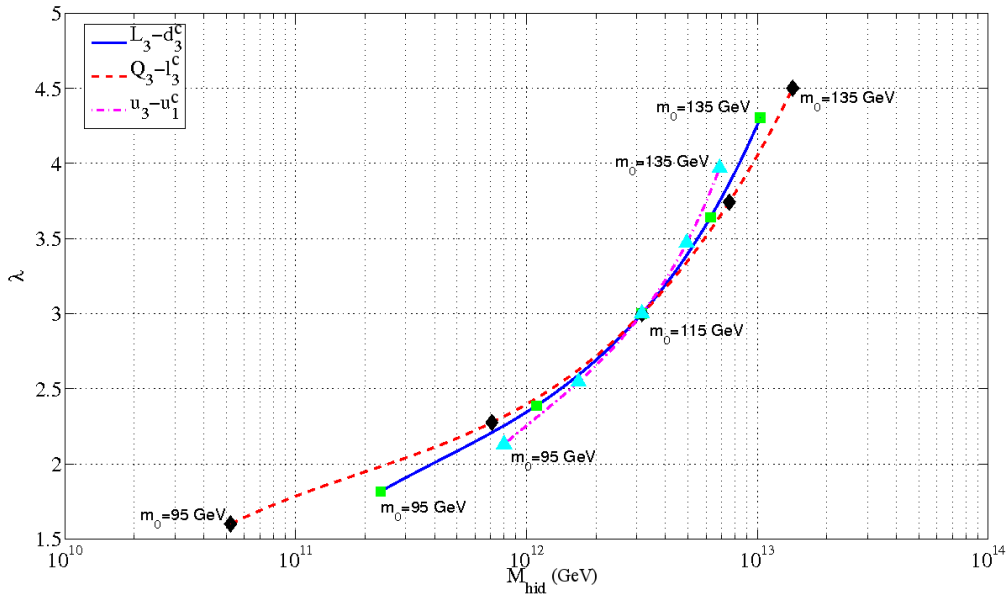


Figure 10: A consistency check on the contour intersection shown in Fig. 9 is possible using a third set of low-energy data. In this example,  $m_0 = 115 \text{ GeV}$ ,  $\lambda = 3$ , and  $M_{hid} = 3.16 \times 10^{12} \text{ GeV}$ .

the hidden-sector parameters. In general, these two determinations of the hidden-sector parameters will agree only if we are reconstructing correctly the model parametrization of the hidden-sector dynamics. As such, with the two independent determinations, we can determine both the correct parametrization of the hidden sector, and fit its parameters with a redundant check.

### 4.3 General Reconstruction Strategy

These two examples demonstrate a general strategy that can be employed with the low-energy data to determine model parameters of the hidden sector, which we summarize as follows:

- Using the measured low-energy data on the soft supersymmetry-breaking scalar masses, run the MSSM RGEs bottom-up and check for the appearance of a mirage scalar unification scale, distinct from the gauge coupling unification scale,  $M_X$ . Mirage scalar unification would signify the potential presence of a hidden-sector

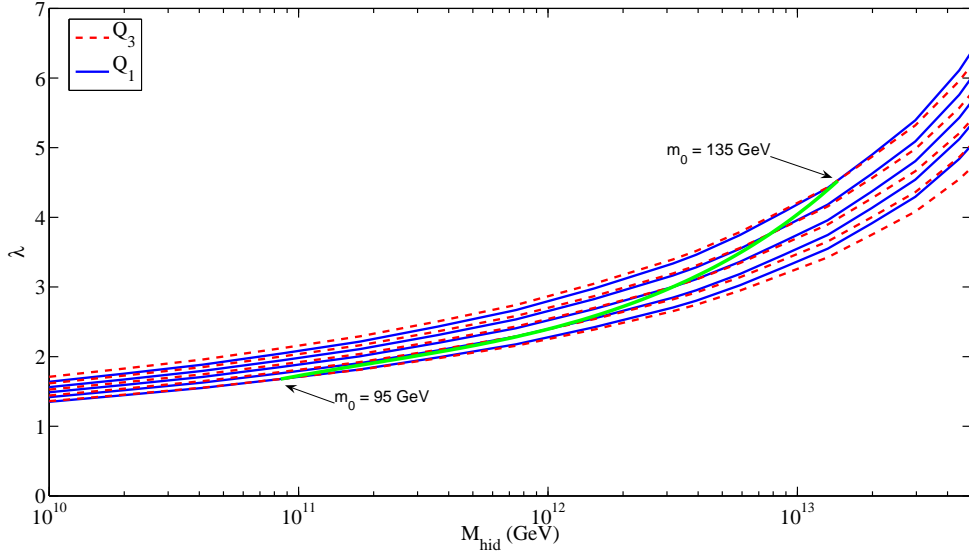


Figure 11: *Overlay of the contours of  $Q_1$  and  $Q_3$  masses, assuming only that they have a common scalar mass at the input scale.*

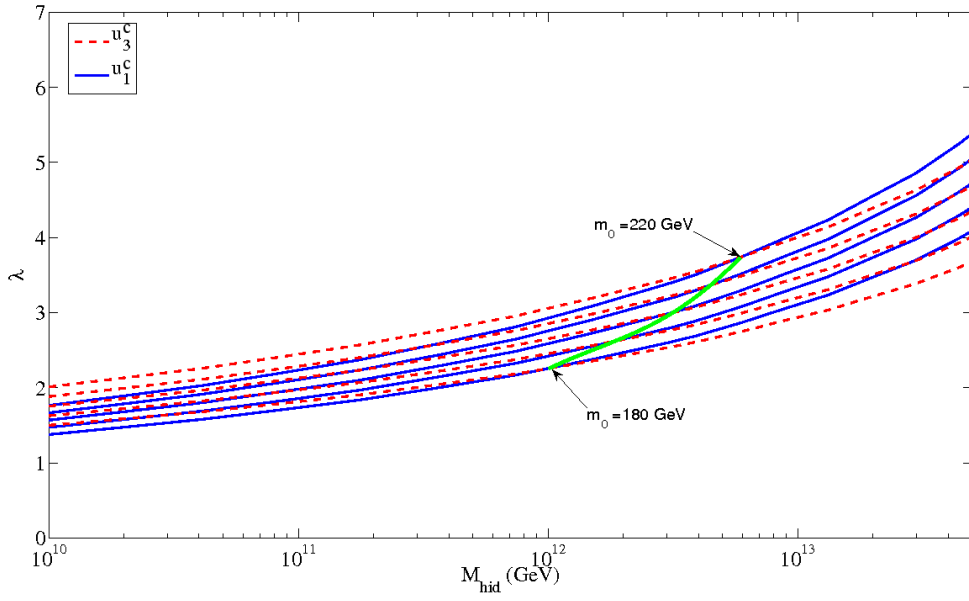


Figure 12: *Overlay of the contours of the  $u_1^c$  and  $u_3^c$  masses, assuming only that they have a common scalar mass at the input scale.*

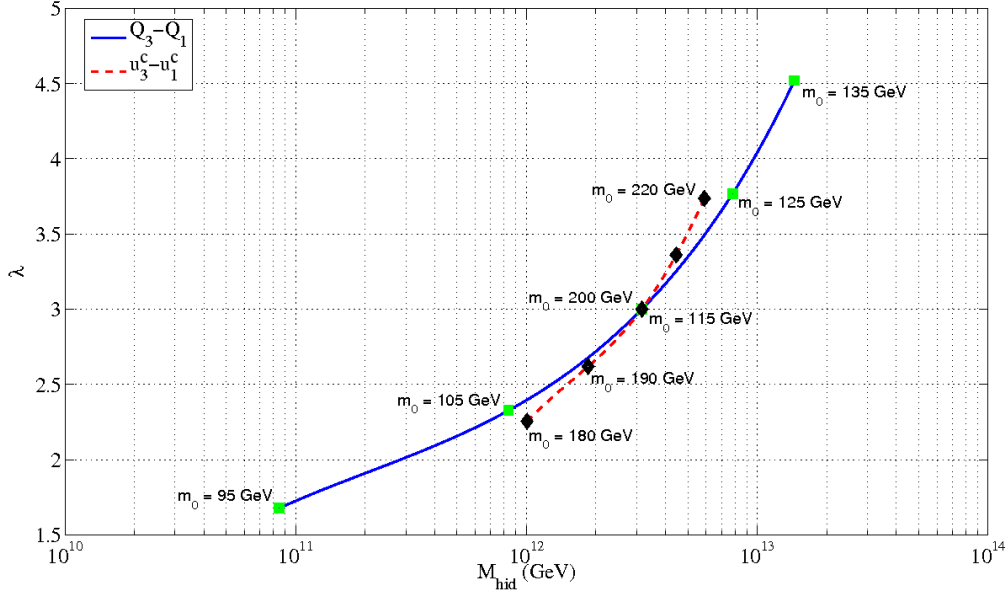


Figure 13: *Intersection of the intersection curves from the previous two figures, yielding consistent parameters of the hidden sector reconstructed from the low-energy data. We allow  $m'_0 \neq m_0$  in this example.*

effect.

- Starting with the contours in the  $Q_3 - Q_1$  and  $u_3^c - u_1^c$  systems constructed, as described above, from a model of the hidden sector together with the conservative assumption of common scalar masses among particles with the same gauge quantum numbers, construct the curves of intersection and overlay them in the  $M_{hid}-\lambda$  plane. Using the  $Q_3 - Q_1$  and  $u_3^c - u_1^c$  system takes advantage of the large top Yukawa coupling, which provides the largest generational splitting in the RGE flow.
- If  $\tan\beta$  is sufficiently large (which in practice is determined by the following procedure yielding a definite result), starting with contours in the  $Q_3 - Q_1$  and  $d_3^c - d_1^c$  systems constructed from a model of the hidden sector together with the conservative assumption of common scalar masses among particles with the same gauge quantum numbers, construct the curves of intersection and overlay them in the  $M_{hid}-\lambda$  plane. Using the  $Q_3 - Q_1$  and  $d_3^c - d_1^c$  system takes advantage of the potentially large (enhanced at  $\tan\beta$ ) bottom Yukawa coupling, which provides the

second-largest generational splitting in the RGE flow. Try both this step and the previous one for each of the different hidden-sector parametrizations; the hidden-sector parametrization which most correctly represents the qualitative behaviour of the hidden sector renormalization effects will be the one for which the two parameter determinations best agree. This then determines both the correct parametrization for the hidden sector and gives a redundant determination of the parameters.

- For the intersections established in the previous steps, the affine parameter along each curve will yield the common scalar mass for each system at the intersection point, but these could be different for the two curves in the intersections of lines of intersection. If the extracted common scalar masses are the same for both systems (in each of the reconstructions proposed above if both are feasible), this would indicate that all scalar particles may have universal masses.
- If the  $Q_3 - Q_1$  and  $u_3^c - u_1^c$  system yields the same common scalar mass at intersection (and the  $Q_3 - Q_1$  and  $d_3^c - d_1^c$  system does likewise, assuming that this reconstruction is feasible) apply the universality assumption using the parameters determined from the  $Q_3 - Q_1$  and  $u_3^c - u_1^c$  system (and  $Q_3 - Q_1$  and  $d_3^c - d_1^c$  system if it is feasible and in agreement) and predict  $l_{(12)}$ ;  $l_3^c$ <sup>5</sup>. In the case of a successful prediction, we would have a completely self-consistent model of the hidden sector with knowledge of the boundary conditions for the scalar masses at the true unification scale. If the prediction does not yield a successful prediction, then either the assumption on universality is incorrect or potentially the model of the hidden sector is wrong, in the case that one was not able to do the redundant check using the  $Q_3 - Q_1$  and  $d_3^c - d_1^c$  system. (In this case, we can repeat the process with a different model of the hidden sector.)

---

<sup>5</sup>We note that  $L_{(12)}$ ;  $L_3$  are in general affected by renormalization effects associated with the seesaw interactions, as are  $N_{(12)}$ ;  $N_3$ ; we discuss hidden-sector effects and the seesaw mechanism in a companion paper.

## 5 Reconstruction Algorithm

We now review the steps that would be needed, starting from experimental measurements, to characterize and parametrize the hidden sector, following the approach proposed in the previous section.

Clearly all of the above considerations are moot if the LHC does not actually discover supersymmetry. However, it is important not only that the LHC finds some evidence for supersymmetry, in the form of certain superpartners, but also that the LHC measures the masses of sufficiently many of the spartners of Standard Model particles to be able to make redundant consistency checks. It is also important to know whether any other chiral multiplets carrying Standard Model charges appear below the GUT scale. Our analysis above was dependent on the RGE running of the MSSM parameters between the high scales of mediation and the hidden sector on one hand, and the electroweak scale on the other hand, and we assumed there is a large desert in between. To be able to extrapolate reliably through the desert, we need to know the entire matter content of the effective theory at desert energies.

In particular, to use our algorithm we need to assume that the LHC (if necessary in combination with a linear  $e^+e^-$  collider) is able to determine the complete superspectrum below the desert. This is a necessary input into any determination of gauge-coupling unification in supersymmetric extensions of the Standard Model. The MSSM has the feature that RGE extrapolation based on its particle content yields gauge-coupling unification at a unification scale of order  $10^{16}$  GeV. With the LHC, we trust that we will no longer be assuming some low-energy field particle content, but rather we will be in a position to determine it from experiment. To get the extrapolation right, and really be able to test gauge-coupling unification, we need to know the complete list of supermultiplets which are dynamical at desert energies. In addition, one would also like to reduce the (controllable) theory uncertainties as much as possible: these include, in particular, higher-order terms in the  $\beta$  functions for the RGE running, and the TeV-scale threshold corrections for the observed spectrum of input masses, which should also be incorporated at high order.

If, after the complete spectrum of superpartners and their physical masses has been

determined, one finds that the gauge-coupling extrapolation does indeed lead to unification at a large scale of  $\mathcal{O}(10^{16})$  GeV, one can then ask about the gauginos and scalars. As we have discussed above, gauginos receive mass renormalization from the hidden-sector only through external-line wave function renormalization of the singlet superfield whose F-term is responsible for supersymmetry breaking. If we adopt a renormalization prescription in which this wave-function renormalization is absorbed into the VEV, then the effects of the renormalization on all the soft masses can be absorbed into a common rescaling of the boundary value at the mediation scale, and in this renormalization scheme the gauginos are not directly affected by the hidden sector.

This means that the gauginos give a clean characterization of the high-scale mechanisms of supersymmetry mediation and breaking, unobscured by hidden-sector effects. The generality and simplicity of the patterns of gaugino masses that may arise in modern supersymmetric unified theories has been emphasized in the review [20]. By comparing the gaugino mass pattern observed at the LHC (and possibly a linear collider) to these theoretical expectations, one may get an indication of the model classes preferred by the data. This would in turn give some indication of the expectations we may have for the high-scale scalar masses input at the mediation or unification scale.

In order to try to use hidden-sector effects on the scalar masses to observe the dynamics of the hidden sector, a key question will be the degree of scalar-mass universality. Universality of the sfermions with identical Standard Model gauge charges seems very plausible [12, 13, 15, 14], but will need to be checked. Many more consistency checks would be possible if there is a higher degree of scalar-mass universality, as in certain GUTs or the CMSSM. In order to check these hypotheses, one will need to measure the mass-squared parameters for the scalars of different gauge charges, and separately for the squarks and sleptons of the third generation. Doing this precisely will presumably necessitate studying the scalars not only at the LHC, but also at a linear  $e^+e^-$  collider, such as CLIC, capable of producing all the scalars of the supersymmetric extension of the Standard Model, especially including the squarks which are the starting point of our reconstruction algorithm.

The precision of an  $e^+e^-$  collider will be important, as the scalar masses-squared that we use in our reconstruction are only parts of entries in the mass-squared matrix for

the chiral scalars that are the partners of the left- and right-handed quarks or leptons. One will need to fix the other entries in the mass-squared matrix from data, and that will necessitate fixing several of the soft supersymmetry-breaking parameters, including A-terms. It will also be necessary to determine  $\tan\beta$  quite accurately. The required level of detail and precision will be hard to achieve without combining LHC studies with follow-up precision studies at an  $e^+e^-$  collider.

We note that the reconstruction procedure outlined in the previous section was exemplified on the basis of scalars with a general pattern we may characterize as gravity/modulus mediated. That was not essential to the reconstruction; mirage/anomaly mediation patterns of high-scale input scalar masses would have been equally adapted to our arguments. One can use the gaugino mass patterns from the previous paragraph to infer the type of unification theory, and hence the type of input pattern to consider. It will be checked *a posteriori* by success in finding a consistent set of hidden-sector parameters that matches the input pattern of scalar masses within the class of models.

Also, with a given pattern of input scalar masses (e.g., universal as in pure gravity mediation) there will be linear combinations of the low-energy scalar mass parameters which are not affected by the hidden-sector renormalization (at leading order in the observable-sector couplings). These sum rules can be used to test whether the observed distortion of the scalar spectrum is due in fact to hidden-sector effects and not some other new high-scale physics. We enumerate these sum rules in Appendix A, for the case of universal scalar masses (see also [10]). We note that, beyond leading order, RGE feedback from observable-sector interactions will spread the hidden-sector effects through all the soft parameters, so that complete simultaneous fits to the soft parameters (gaugino masses included) would be essential.

## 6 Conclusions

We have demonstrated in this paper that it is possible, in principle, to extract dynamical parameters of the hidden sector responsible for supersymmetry breaking from measurements of sparticle masses in the observable sector. Hidden-sector dynamics could affect the renormalization of soft supersymmetry-breaking scalar masses between the input scale

$M_X$  and the hidden-sector scale  $M_{Hid}$ . This extra renormalization would make it seem as if observable squark and slepton masses would unify at some ‘mirage’ scale below  $M_X$ , if only the MSSM RGEs were used to run upwards. We showed how the parameters of the hidden sector could be measured using low-energy data, and consistency checks performed. We demonstrated the procedure in two examples, one assuming total universality of the soft supersymmetry-breaking scalar masses, and one assuming universality only for sfermions with the same gauge quantum numbers, and gave a general prescription for extracting dynamical parameters of the hidden sector.

Several aspects of this programme require further study. It is unclear whether LHC measurements by themselves would provide enough low-energy information, and we anticipate that information from a linear collider would also be required: its precision and ability to determine slepton mass parameters would both be important for our programme. We have not quantified the accuracy with which soft supersymmetry-breaking masses should be measured in order to obtain interesting accuracy in the hidden-sector parameters. This might actually be premature in the absence of a credible model of the hidden sector to use as a benchmark. Also, we have not included higher-order terms in the RGEs for the soft supersymmetry-breaking parameters: this is important to do, though we do not expect our essential conclusions to be altered significantly. Finally, we note that it would be interesting to extend the approach described here to lower-scale models of supersymmetry breaking, such as gauge mediation.

We hope that this work opens the way to further studies of the possibility of measuring observable effects of the hidden-sector dynamics. The basic motivation for such a programme is clear. There is certainly no shortage of scope for further studies, and in a companion paper [11] we explore some possible implications of the hidden sector for flavour studies, particularly in the lepton sector. Perhaps the concept of hidden-sector phenomenology is not an oxymoron.

## Acknowledgments

We are deeply grateful to Graham Ross for sharing with us the parametrization of hidden sector renormalization effects which we have employed in Section 3 of this work, as well as

for helpful discussions and encouragement. We would like to thank John March-Russell and Stephen West for useful discussions. We would also like to acknowledge the support of the Natural Sciences and Engineering Research Council of Canada.

## Appendix A: Scalar-Mass Sum Rules in the Presence of a Hidden Sector

When hidden-sector renormalization of the scalar mass operator is combined with the observable-sector gauge and Yukawa interactions, there is a distortion of the mass pattern of the scalars at low energies. However, at one-loop order in the visible-sector couplings, and to all orders in the hidden-sector couplings, some relations are preserved [8, 10]. For the case of universal input scalar masses, without further assumptions one has:

$$m_{\tilde{Q}}^2 - 2m_{\tilde{u}^c}^2 + m_{\tilde{d}^c}^2 - m_{\tilde{L}}^2 + m_{\tilde{e}^c}^2 = 0 \quad (29)$$

$$2m_{\tilde{Q}_3}^2 - m_{\tilde{u}_3^c}^2 - m_{\tilde{d}_3^c}^2 - 2m_{\tilde{Q}_1}^2 + m_{\tilde{u}_1^c}^2 + m_{\tilde{d}_1^c}^2 = 0 \quad (30)$$

If  $\tan\beta$  is small one also has:

$$2m_{\tilde{Q}_3}^2 - m_{\tilde{u}_3^c}^2 - 2m_{\tilde{Q}_1}^2 + m_{\tilde{u}_1^c}^2 = 0 \quad (31)$$

$$m_{\tilde{e}_3^c}^2 - m_{\tilde{e}_1^c}^2 = 0 \quad (32)$$

If there are no neutrino seesaw effects visible in the soft masses one also has:

$$2m_{\tilde{L}_3}^2 - m_{\tilde{e}_3^c}^2 - 2m_{\tilde{L}_1}^2 + m_{\tilde{e}_1^c}^2 = 0 \quad (33)$$

If the  $\mu$  term does not arise from a Giudice-Masiero mechanism and  $m_H = m_{\bar{H}}$  one also has:

$$3m_{\tilde{u}_3^c}^2 - 3m_{\tilde{d}_3^c}^2 + 2m_{\tilde{L}_3}^2 - 2m_{\tilde{e}_3^c}^2 - 2m_H^2 + 2m_{\bar{H}}^2 - 3m_{\tilde{u}_1^c}^2 + 3m_{\tilde{d}_1^c}^2 - 2m_{\tilde{L}_1}^2 + 2m_{\tilde{e}_1^c}^2 = 0 \quad (34)$$

If the  $\mu$  term does not arise from a Giudice-Masiero mechanism and  $m_H = m_{\bar{H}} = m_{\tilde{q}} = m_{\tilde{l}}$  one also has:

$$-3m_{\tilde{u}_3^c}^2 - m_{\tilde{e}_3^c}^2 + 2m_H^2 + 3m_{\tilde{d}_1^c}^2 - 2m_{\tilde{L}_1}^2 + m_{\tilde{e}_1^c}^2 = 0 \quad (35)$$

These relations allow one to check the consistency of various assumptions on the soft parameters with RGE evolution including contributions from the hidden sector. Note that they are only true to leading order in the observable-sector interactions.

# Appendix B: MSSM Soft Supersymmetry-Breaking Parameter RGEs From One-Loop Observable-Sector Contributions

In this Appendix we present the one-loop MSSM RGEs including gauge-singlet Majorana neutrinos. Hidden-sector contributions to the RGE flow should be added to these (for the soft scalar mass-squared terms) following the discussion in Sections 3 and 4 of the text.

$$\frac{dX}{dt} = \frac{1}{16\pi^2} \dot{X} \quad (36)$$

where  $X$  denotes any of  $g_1, g_2, g_3, \mathbf{Y}_\nu, \mathbf{Y}_e, \mathbf{Y}_u, \mathbf{Y}_d, M_1, M_2, M_3, m_{H_u}^2, m_{H_d}^2, \mathbf{m}_L^2, \mathbf{m}_\nu^2, \mathbf{m}_{e^c}^2, \mathbf{m}_q^2, \mathbf{m}_{u^c}^2, \mathbf{m}_{d^c}^2, \mathbf{A}_\nu, \mathbf{A}_e, \mathbf{A}_u, \mathbf{A}_d$ . The dotted quantities appear below:

$$\dot{g}_1 = 11g_1^3, \quad (37)$$

$$\dot{g}_2 = g_2^3, \quad (38)$$

$$\dot{g}_3 = -3g_3^3, \quad (39)$$

$$(40)$$

Yukawa couplings

$$\dot{\mathbf{Y}}_\nu = \mathbf{Y}_\nu \left( -g_1^2 \mathbf{I} - 3g_2^2 \mathbf{I} + 3\text{Tr}(\mathbf{Y}_u^\dagger \mathbf{Y}_u) \mathbf{I} + \text{Tr}(\mathbf{Y}_\nu^\dagger \mathbf{Y}_\nu) \mathbf{I} + 3\mathbf{Y}_\nu^\dagger \mathbf{Y}_\nu + \mathbf{Y}_e^\dagger \mathbf{Y}_e \right), \quad (41)$$

$$\dot{\mathbf{Y}}_e = \mathbf{Y}_e \left( -3g_1^2 \mathbf{I} - 3g_2^2 \mathbf{I} + 3\text{Tr}(\mathbf{Y}_d^\dagger \mathbf{Y}_d) \mathbf{I} + \text{Tr}(\mathbf{Y}_e^\dagger \mathbf{Y}_e) \mathbf{I} + 3\mathbf{Y}_e^\dagger \mathbf{Y}_e + \mathbf{Y}_\nu^\dagger \mathbf{Y}_\nu \right), \quad (42)$$

$$\begin{aligned} \dot{\mathbf{Y}}_u = & \mathbf{Y}_u \left( -\frac{13}{9}g_1^2 \mathbf{I} - 3g_2^2 \mathbf{I} - \frac{16}{3}g_3^2 \mathbf{I} + 3\text{Tr}(\mathbf{Y}_u^\dagger \mathbf{Y}_u) \mathbf{I} + \text{Tr}(\mathbf{Y}_\nu^\dagger \mathbf{Y}_\nu) \mathbf{I} \right. \\ & \left. + 3\mathbf{Y}_u^\dagger \mathbf{Y}_u + \mathbf{Y}_d^\dagger \mathbf{Y}_d \right), \end{aligned} \quad (43)$$

$$\begin{aligned} \dot{\mathbf{Y}}_d = & \mathbf{Y}_d \left( -\frac{7}{9}g_1^2 \mathbf{I} - 3g_2^2 \mathbf{I} - \frac{16}{3}g_3^2 \mathbf{I} + 3\text{Tr}(\mathbf{Y}_d^\dagger \mathbf{Y}_d) \mathbf{I} + \text{Tr}(\mathbf{Y}_e^\dagger \mathbf{Y}_e) \mathbf{I} \right. \\ & \left. + 3\mathbf{Y}_d^\dagger \mathbf{Y}_d + \mathbf{Y}_u^\dagger \mathbf{Y}_u \right), \end{aligned} \quad (44)$$

$$\dot{M}_1 = 22g_1^2 M_1, \quad (45)$$

$$\dot{M}_2 = 2g_2^2 M_2, \quad (46)$$

$$\dot{M}_3 = -6g_3^2 M_3, \quad (47)$$

$$S = m_{H_u}^2 - m_{H_d}^2 + \text{Tr} \left( \mathbf{m}_{\tilde{q}}^2 - 2\mathbf{m}_{\tilde{u}^c}^2 + \mathbf{m}_{\tilde{d}^c}^2 - \mathbf{m}_{\tilde{L}}^2 + \mathbf{m}_{\tilde{e}^c}^2 \right), \quad (48)$$

up and down Higgs soft masses

$$\begin{aligned} \dot{m}_{H_u}^2 &= 6\text{Tr} \left( \mathbf{m}_{\tilde{q}}^2 \mathbf{Y}_u^\dagger \mathbf{Y}_u + \mathbf{Y}_u^\dagger \mathbf{m}_{\tilde{u}^c}^2 \mathbf{Y}_u + m_{H_u}^2 \mathbf{Y}_u^\dagger \mathbf{Y}_u + \mathbf{A}_u^\dagger \mathbf{A}_u \right) \\ &\quad + 2\text{Tr} \left( \mathbf{m}_{\tilde{L}}^2 \mathbf{Y}_\nu^\dagger \mathbf{Y}_\nu + \mathbf{Y}_\nu^\dagger \mathbf{m}_{\tilde{\nu}}^2 \mathbf{Y}_\nu + m_{H_u}^2 \mathbf{Y}_\nu^\dagger \mathbf{Y}_\nu + \mathbf{A}_\nu^\dagger \mathbf{A}_\nu \right) \\ &\quad - 2g_1^2 M_1^2 - 6g_2^2 M_2^2 + g_1^2 S + (2\lambda^2 m_{H_u}^2), \end{aligned} \quad (49)$$

$$\begin{aligned} \dot{m}_{H_d}^2 &= 2\text{Tr} \left( \mathbf{m}_{\tilde{L}}^2 \mathbf{Y}_e^\dagger \mathbf{Y}_e + \mathbf{Y}_e^\dagger \mathbf{m}_{\tilde{e}^c}^2 \mathbf{Y}_e + m_{H_d}^2 \mathbf{Y}_e^\dagger \mathbf{Y}_e + \mathbf{A}_e^\dagger \mathbf{A}_e \right) \\ &\quad + 6\text{Tr} \left( \mathbf{m}_{\tilde{q}}^2 \mathbf{Y}_d^\dagger \mathbf{Y}_d + \mathbf{Y}_d^\dagger \mathbf{m}_{\tilde{d}^c}^2 \mathbf{Y}_d + m_{H_d}^2 \mathbf{Y}_d^\dagger \mathbf{Y}_d + \mathbf{A}_d^\dagger \mathbf{A}_d \right) \\ &\quad - 2g_1^2 M_1^2 - 6g_2^2 M_2^2 - g_1^2 S + (2\lambda^2 m_{H_d}^2), \end{aligned} \quad (50)$$

$$\begin{aligned} \dot{\mathbf{m}}_{\tilde{L}}^2 &= \mathbf{m}_{\tilde{L}}^2 \mathbf{Y}_e^\dagger \mathbf{Y}_e + \mathbf{Y}_e^\dagger \mathbf{Y}_e \mathbf{m}_{\tilde{L}}^2 + \mathbf{m}_{\tilde{L}}^2 \mathbf{Y}_\nu^\dagger \mathbf{Y}_\nu + \mathbf{Y}_\nu^\dagger \mathbf{Y}_\nu \mathbf{m}_{\tilde{L}}^2 \\ &\quad + 2\mathbf{Y}_e^\dagger \mathbf{m}_{\tilde{e}^c}^2 \mathbf{Y}_e + 2m_{H_d}^2 \mathbf{Y}_e^\dagger \mathbf{Y}_e + 2\mathbf{A}_e^\dagger \mathbf{A}_e \\ &\quad + 2\mathbf{Y}_\nu^\dagger \mathbf{m}_{\tilde{\nu}}^2 \mathbf{Y}_\nu + 2m_{H_u}^2 \mathbf{Y}_\nu^\dagger \mathbf{Y}_\nu + 2\mathbf{A}_\nu^\dagger \mathbf{A}_\nu \\ &\quad - 2g_1^2 M_1^2 \mathbf{I} - 6g_2^2 M_2^2 \mathbf{I} - g_1^2 S \mathbf{I} + (2\lambda^2 \mathbf{m}_{\tilde{L}}^2), \end{aligned} \quad (51)$$

$$\dot{\mathbf{m}}_{\tilde{\nu}}^2 = 2\mathbf{m}_{\tilde{\nu}}^2 \mathbf{Y}_\nu \mathbf{Y}_\nu^\dagger + 2\mathbf{Y}_\nu \mathbf{Y}_\nu^\dagger \mathbf{m}_{\tilde{\nu}}^2 + 4\mathbf{Y}_\nu \mathbf{m}_{\tilde{L}}^2 \mathbf{Y}_\nu^\dagger + 4m_{H_u}^2 \mathbf{Y}_\nu \mathbf{Y}_\nu^\dagger + 4\mathbf{A}_\nu \mathbf{A}_\nu^\dagger + (2\lambda^2 \mathbf{m}_{\tilde{\nu}}^2), \quad (52)$$

$$\begin{aligned} \dot{\mathbf{m}}_{\tilde{e}^c}^2 &= 2\mathbf{m}_{\tilde{e}^c}^2 \mathbf{Y}_e \mathbf{Y}_e^\dagger + 2\mathbf{Y}_e \mathbf{Y}_e^\dagger \mathbf{m}_{\tilde{e}^c}^2 + 4\mathbf{Y}_e \mathbf{m}_{\tilde{L}}^2 \mathbf{Y}_e^\dagger + 4m_{H_d}^2 \mathbf{Y}_e \mathbf{Y}_e^\dagger + 4\mathbf{A}_e \mathbf{A}_e^\dagger \\ &\quad - 8g_1^2 M_1^2 \mathbf{I} + 2g_1^2 S \mathbf{I} + (2\lambda^2 \mathbf{m}_{\tilde{e}^c}^2), \end{aligned} \quad (53)$$

$$\begin{aligned} \dot{\mathbf{m}}_{\tilde{q}}^2 &= \mathbf{m}_{\tilde{q}}^2 \mathbf{Y}_u^\dagger \mathbf{Y}_u + \mathbf{Y}_u^\dagger \mathbf{Y}_u \mathbf{m}_{\tilde{q}}^2 + 2\mathbf{Y}_u^\dagger \mathbf{m}_{\tilde{u}^c}^2 \mathbf{Y}_u + 2m_{H_u}^2 \mathbf{Y}_u^\dagger \mathbf{Y}_u + 2\mathbf{A}_u^\dagger \mathbf{A}_u \\ &\quad + \mathbf{m}_{\tilde{q}}^2 \mathbf{Y}_d^\dagger \mathbf{Y}_d + \mathbf{Y}_d^\dagger \mathbf{Y}_d \mathbf{m}_{\tilde{q}}^2 + 2\mathbf{Y}_d^\dagger \mathbf{m}_{\tilde{d}^c}^2 \mathbf{Y}_d + 2m_{H_d}^2 \mathbf{Y}_d^\dagger \mathbf{Y}_d + 2\mathbf{A}_d^\dagger \mathbf{A}_d \\ &\quad - \frac{2}{9}g_1^2 M_1^2 \mathbf{I} - 6g_2^2 M_2^2 \mathbf{I} - \frac{32}{3}g_3^2 M_3^2 \mathbf{I} + \frac{1}{3}g_1^2 S \mathbf{I} + (2\lambda^2 \mathbf{m}_{\tilde{q}}^2), \end{aligned} \quad (54)$$

$$\begin{aligned} \dot{\mathbf{m}}_{\tilde{u}^c}^2 &= 2\mathbf{m}_{\tilde{u}^c}^2 \mathbf{Y}_u \mathbf{Y}_u^\dagger + 2\mathbf{Y}_u \mathbf{Y}_u^\dagger \mathbf{m}_{\tilde{u}^c}^2 + 4\mathbf{Y}_u \mathbf{m}_{\tilde{q}}^2 \mathbf{Y}_u^\dagger + 4m_{H_u}^2 \mathbf{Y}_u \mathbf{Y}_u^\dagger + 4\mathbf{A}_u \mathbf{A}_u^\dagger \\ &\quad - \frac{32}{9}g_1^2 M_1^2 \mathbf{I} - \frac{32}{3}g_3^2 M_3^2 \mathbf{I} - \frac{4}{3}g_1^2 S \mathbf{I} + (2\lambda^2 \mathbf{m}_{\tilde{u}^c}^2), \end{aligned} \quad (55)$$

$$\begin{aligned} \dot{\mathbf{m}}_{\tilde{d}^c}^2 &= 2\mathbf{m}_{\tilde{d}^c}^2 \mathbf{Y}_d \mathbf{Y}_d^\dagger + 2\mathbf{Y}_d \mathbf{Y}_d^\dagger \mathbf{m}_{\tilde{d}^c}^2 + 4\mathbf{Y}_d \mathbf{m}_{\tilde{q}}^2 \mathbf{Y}_d^\dagger + 4m_{H_d}^2 \mathbf{Y}_d \mathbf{Y}_d^\dagger + 4\mathbf{A}_d \mathbf{A}_d^\dagger \\ &\quad - \frac{8}{9}g_1^2 M_1^2 \mathbf{I} - \frac{32}{3}g_3^2 M_3^2 \mathbf{I} + \frac{2}{3}g_1^2 S \mathbf{I} + (2\lambda^2 \mathbf{m}_{\tilde{d}^c}^2), \end{aligned} \quad (56)$$

$$\begin{aligned}
\dot{\mathbf{A}}_\nu &= -g_1^2 \mathbf{A}_\nu - 3g_2^2 \mathbf{A}_\nu + 3\text{Tr}(\mathbf{Y}_u^\dagger \mathbf{Y}_u) \mathbf{A}_\nu + \text{Tr}(\mathbf{Y}_\nu^\dagger \mathbf{Y}_\nu) \mathbf{A}_\nu \\
&\quad - 2g_1^2 M_1 \mathbf{Y}_\nu - 6g_2^2 M_2 \mathbf{Y}_\nu + 6\text{Tr}(\mathbf{Y}_u^\dagger \mathbf{A}_u) \mathbf{Y}_\nu + 2\text{Tr}(\mathbf{Y}_\nu^\dagger \mathbf{A}_\nu) \mathbf{Y}_\nu \\
&\quad + 4\mathbf{Y}_\nu \mathbf{Y}_\nu^\dagger \mathbf{A}_\nu + 5\mathbf{A}_\nu \mathbf{Y}_\nu^\dagger \mathbf{Y}_\nu + 2\mathbf{Y}_\nu \mathbf{Y}_e^\dagger \mathbf{A}_e + \mathbf{A}_\nu \mathbf{Y}_e^\dagger \mathbf{Y}_e,
\end{aligned} \tag{57}$$

$$\begin{aligned}
\dot{\mathbf{A}}_e &= -3g_1^2 \mathbf{A}_e - 3g_2^2 \mathbf{A}_e + 3\text{Tr}(\mathbf{Y}_d^\dagger \mathbf{Y}_d) \mathbf{A}_e + \text{Tr}(\mathbf{Y}_e^\dagger \mathbf{Y}_e) \mathbf{A}_e \\
&\quad - 6g_1^2 M_1 \mathbf{Y}_e - 6g_2^2 M_2 \mathbf{Y}_e + 6\text{Tr}(\mathbf{Y}_d^\dagger \mathbf{A}_d) \mathbf{Y}_e + 2\text{Tr}(\mathbf{Y}_e^\dagger \mathbf{A}_e) \mathbf{Y}_e \\
&\quad + 4\mathbf{Y}_e \mathbf{Y}_e^\dagger \mathbf{A}_e + 5\mathbf{A}_e \mathbf{Y}_e^\dagger \mathbf{Y}_e + 2\mathbf{Y}_e \mathbf{Y}_\nu^\dagger \mathbf{A}_\nu + \mathbf{A}_e \mathbf{Y}_\nu^\dagger \mathbf{Y}_\nu,
\end{aligned} \tag{58}$$

$$\begin{aligned}
\dot{\mathbf{A}}_u &= -\frac{13}{9}g_1^2 \mathbf{A}_u - 3g_2^2 \mathbf{A}_u - \frac{16}{3}g_3^2 \mathbf{A}_u + 3\text{Tr}(\mathbf{Y}_u^\dagger \mathbf{Y}_u) \mathbf{A}_u + \text{Tr}(\mathbf{Y}_\nu^\dagger \mathbf{Y}_\nu) \mathbf{A}_u \\
&\quad - \frac{26}{9}g_1^2 M_1 \mathbf{Y}_u - 6g_2^2 M_2 \mathbf{Y}_u - \frac{32}{3}g_3^2 M_3 \mathbf{Y}_u + 6\text{Tr}(\mathbf{Y}_u^\dagger \mathbf{A}_u) \mathbf{Y}_u + 2\text{Tr}(\mathbf{Y}_\nu^\dagger \mathbf{A}_\nu) \mathbf{Y}_u \\
&\quad + 4\mathbf{Y}_u \mathbf{Y}_u^\dagger \mathbf{A}_u + 5\mathbf{A}_u \mathbf{Y}_u^\dagger \mathbf{Y}_u + 2\mathbf{Y}_u \mathbf{Y}_d^\dagger \mathbf{A}_d + \mathbf{A}_u \mathbf{Y}_d^\dagger \mathbf{Y}_d,
\end{aligned} \tag{59}$$

$$\begin{aligned}
\dot{\mathbf{A}}_d &= -\frac{7}{9}g_1^2 \mathbf{A}_d - 3g_2^2 \mathbf{A}_d - \frac{16}{3}g_3^2 \mathbf{A}_d + 3\text{Tr}(\mathbf{Y}_d^\dagger \mathbf{Y}_d) \mathbf{A}_d + \text{Tr}(\mathbf{Y}_e^\dagger \mathbf{Y}_e) \mathbf{A}_d \\
&\quad - \frac{14}{9}g_1^2 M_1 \mathbf{Y}_d - 6g_2^2 M_2 \mathbf{Y}_d - \frac{32}{3}g_3^2 M_3 \mathbf{Y}_d + 6\text{Tr}(\mathbf{Y}_d^\dagger \mathbf{A}_d) \mathbf{Y}_d + 2\text{Tr}(\mathbf{Y}_e^\dagger \mathbf{A}_e) \mathbf{Y}_d \\
&\quad + 4\mathbf{Y}_d \mathbf{Y}_d^\dagger \mathbf{A}_d + 5\mathbf{A}_d \mathbf{Y}_d^\dagger \mathbf{Y}_d + 2\mathbf{Y}_d \mathbf{Y}_u^\dagger \mathbf{A}_u + \mathbf{A}_d \mathbf{Y}_u^\dagger \mathbf{Y}_u.
\end{aligned} \tag{60}$$

## References

- [1] J. Polonyi, Central Institute of Research (Budapest) preprint KFKI-77-93 (1977).
- [2] E. Cremmer, B. Julia, J. Scherk, P. van Nieuwenhuizen, S. Ferrara and L. Girardello, Phys. Lett. B **79** (1978) 231.
- [3] E. Cremmer, B. Julia, J. Scherk, S. Ferrara, L. Girardello and P. van Nieuwenhuizen, Nucl. Phys. B **147** (1979) 105.
- [4] H. P. Nilles, Phys. Lett. B **115** (1982) 193.
- [5] J. P. Derendinger, L. E. Ibanez and H. P. Nilles, Phys. Lett. B **155** (1985) 65.
- [6] J. R. Ellis, talk at SUSY07 and arXiv:0710.4959 [hep-ph].
- [7] M. Dine *et al.*, Phys. Rev. **D70** (2004) 045023, arXiv:hep-ph/0405159.

- [8] A. Cohen, T. Roy and M. Schmalz, JHEP **0702** (2007) 027, arXiv:hep-ph/0612100.
- [9] H. Murayama, Y. Nomura and D. Poland, Phys. Rev. **D77** (2008) 015005, arXiv:0709.0775 [hep-ph].
- [10] Y. Kawamura, T. Kinami and T. Miura, arXiv:0810.3965 [hep-ph].
- [11] B. A. Campbell, J. R. Ellis and D. Maybury, CERN-PH-TH/2008-210.
- [12] J. R. Ellis and D. V. Nanopoulos, Phys. Lett. B **110** (1982) 44.
- [13] R. Barbieri and R. Gatto, Phys. Lett. B **110** (1982) 211.
- [14] B. A. Campbell, Phys. Rev. **D28** (1983) 209-216.
- [15] T. Inami and C. S. Lim Nucl. Phys. B **207** (1982) 553.
- [16] L. E. Ibanez, talk at Strings08, and  
L. Aparicio, D. G. Cerdeneo and L. E. Ibanez, arXiv:0805.2943 [hep-ph].
- [17] H. P. Nilles, talk at SUSY08, and arXiv:0809.4390 [hep-th].
- [18] G. G. Ross, unpublished.
- [19] H. Baer, E. K. Park, X. Tata and T. T. Wang, Phys. Lett. B **641** (2006) 447 [arXiv:hep-ph/0607085].
- [20] K. Choi and H. P. Nilles, JHEP **0704** (2007) 006 [hep-ph/0702146].